

# Paleo-ocean chemistry characteristics of the Cryogenian Datangpo Formation in South China and implications for manganese metallogenesis

Zhixin Ma <sup>a,b,\*</sup>, Yun Ling <sup>c</sup>, Yongjun Qin <sup>a,d,\*</sup>, Yu Liu <sup>e</sup>, Xicai Yao <sup>f</sup>, Ping Wang <sup>g</sup>, Xiting Liu <sup>h</sup>

<sup>a</sup> Engineering Technology Innovation Center of Mineral Resources Explorations in Bedrock Zones, Ministry of Natural Resources, Guiyang 550081, China

<sup>b</sup> Chengdu Center, China Geological Survey, Chengdu 610081, China

<sup>c</sup> 607 Geological Party, Chongqing Bureau of Geology and Mineral Exploration and Development, Chongqing 400030, China

<sup>d</sup> Guizhou Provincial Bureau of Geology and Mineral Resources, Guiyang 550004, China

<sup>e</sup> Guizhou Key Laboratory for Strategic Mineral Intelligent Exploration, Guiyang 550000, China

<sup>f</sup> 103 Geological Party, Guizhou Bureau of Geology and Mineral Exploration and Development, Tongren 554300, China

<sup>g</sup> School of Resources and Environment, Henan Polytechnic University, Jiaozuo 454000, China

<sup>h</sup> Key Laboratory of Submarine Geosciences and Prospecting Technology, College of Marine Geosciences, Ocean University of China, Qingdao 266100, China



## ARTICLE INFO

Editor: Bing Shen

### Keywords:

Cryogenian  
Manganese metallogenesis  
Nanhua Basin  
Redox conditions  
Salinity

## ABSTRACT

Paleo-ocean chemical variations play a critical role in understanding the genesis of manganese (Mn) ore deposits within the Cryogenian Datangpo Formation of South China. Based on lithological observations and multiple geochemical proxies—including iron speciation, molybdenum (Mo), uranium (U), vanadium (V), manganese (Mn) concentrations, Sr/Ba ratios, the Chemical Index of Alteration (CIA), and pyrite sulfur isotopes ( $\delta^{34}\text{S}_{\text{py}}$ )—from drill core ZK0602 in Chongqing, South China, the lower black shales of the Datangpo Formation were deposited under euxinic fresh-brackish water conditions and can be subdivided into four intervals (Intervals I, II, III, and IV). Notably, relatively high Mn concentrations and metallogenesis are genetically linked to ferruginous marine conditions in interval II, which is sandwiched between two euxinic fresh-brackish intervals (I and III). An updated conceptual framework is proposed to decipher the co-evolutionary dynamics among redox condition, salinity fluctuations, and manganese metallogenesis. During intervals I and III, Sturtian deglaciation-driven warming enhanced chemical weathering, increasing terrigenous input to the basin and reducing water-column salinity. Concurrently, elevated nutrient inputs from both open-ocean and terrigenous sources heightened surface-water primary productivity and subsequent anaerobic organic matter mineralization in the water column, inducing bottom-water sulfidization and promoting pyrite formation. In contrast, during interval II, as glacial stadials emerged within the interglacial period, chemical weathering weakened, terrigenous input decreased, and the salinity of the basin water body rose to marine levels. Diminished nutrient supplies from both oceanic and terrestrial sources decreased primary productivity, reducing the downward flux of organic matter and sulfate. This shift favored manganese reduction as the dominant organic matter oxidation pathway. Under ferruginous conditions, Mn ore precipitated near the water-sediment interface.

## 1. Introduction

The Neoproterozoic Era (1000–542 Ma) was a crucial geological period marked by two significant glaciations (Hoffman et al., 1998; Pierrehumbert et al., 2011; Spence et al., 2016), dynamic oceanic redox perturbations (Cheng et al., 2021; Song et al., 2023), and the expansion of eukaryotic life (Sahoo et al., 2016; Halverson et al., 2020). Fluctuations in marine oxygen levels during the Neoproterozoic not only

profoundly influenced eukaryotic diversification (Hoshino et al., 2017) and the radiation of animals (Grey et al., 2003; Love et al., 2009), but also played a pivotal role in the genesis of diverse sedimentary minerals. These include the phosphatic deposits of the Ediacaran (Drummond et al., 2016; Qi et al., 2023) and manganese ore bodies in the basal Cryogenian Datangpo Formation (Yu et al., 2019; Ye et al., 2024).

As the redox state of the Datangpo Formation during Cryogenian interglacial periods is critical for deciphering eukaryotic evolution and

\* Corresponding authors at: Engineering Technology Innovation Center of Mineral Resources Explorations in Bedrock Zones, Ministry of Natural Resources, Guiyang 550081, China.

E-mail addresses: zhixinma83@126.com (Z. Ma), 756068385@qq.com (Y. Qin).

the genesis of large-scale manganese ore (Och and Shields-Zhou, 2012; Zhou et al., 2016; Zhou et al., 2022), extensive researches have been conducted on the paleo-ocean redox conditions of the Datangpo Formation through multi-proxy analyses (redox-sensitive elements, iron speciation, and molybdenum/iron/nitrogen isotopes) across diverse stratigraphic sections and drill cores (Li et al., 2012; Zhang et al., 2015; Cheng et al., 2018; Cheng et al., 2021; Wu et al., 2024). Generally, these studies demonstrate that the lower Datangpo Formation was characterized by sulfidic environments intercalated with minor ferruginous episodes (Cheng et al., 2021), with a systematic decrease in anoxic severity upward through the succession (Li et al., 2012; Zhang et al., 2015). However, alternative studies propose that the deep Nanhua Basin underwent episodic ventilation events analogous to modern-day Baltic Sea dynamics (Yu et al., 2016; Ai et al., 2021).

These divergent perspectives on the Nanhua Basin's chemical conditions have constrained mechanistic understanding the metallogenic model of manganese deposits during this critical interval. Moreover, prior researches have predominantly concentrated on the sections in the southern part of Nanhua Basin (e.g., Guizhou Province and Hunan Province) (Yu et al., 2016; Tu et al., 2024; Wang et al., 2024), while relatively few studies have been conducted on the northern part of the Nanhua Basin (e.g., Chongqing City) (Ma et al., 2019). In addition, salinity has been thought to substantially influence oceanic chemical evolution via regulating seawater circulation in response to climatic and hydrologic changes (Remírez and Algeo, 2020; Cao et al., 2023).

However, researches on the relationship between the salinity variations, paleoclimatic evolution and manganese mineralization of the Datangpo Formation is relatively weak (Cheng et al., 2021; Cai et al., 2022; Cao et al., 2024; Wei et al., 2024).

To further constrain the oceanic redox and salinity conditions during the deposition of the basal Datangpo Formation (Cryogenian), this study presents a multi-proxy lithological and geochemical dataset from black shales intercalated with manganese ores in drill core ZK0602, in Chongqing City, in the northern part of Nanhua Basin (Fig. 1). Analytical approaches include redox-sensitive elements (U, Mo, V), iron speciation, Mn, Sr, Ba, the chemical index of alteration (CIA), and pyrite sulfur isotopes ( $\delta^{34}\text{S}_{\text{Py}}$ ). By integrating these data with previous studies on other manganese ore-bearing sections, we propose a conceptual model for manganese metallogenesis in the basal Datangpo Formation of the Nanhua Basin, which is linked to transient seawater redox and salinity fluctuations.

## 2. Geological setting

The South China Block consists of the Yangtze and Cathaysia blocks, which amalgamated during the Sibao orogeny approximately 1000 to 900 million years ago (Li et al., 2002; Li et al., 2009). This region subsequently underwent rifting between 820 Ma and 542 Ma, forming the Nanhua Rift Basin (Wang and Li, 2003; Wang et al., 2009). The Nanhua Rift Basin comprises Wuling and Xuefeng secondary rift basins, along

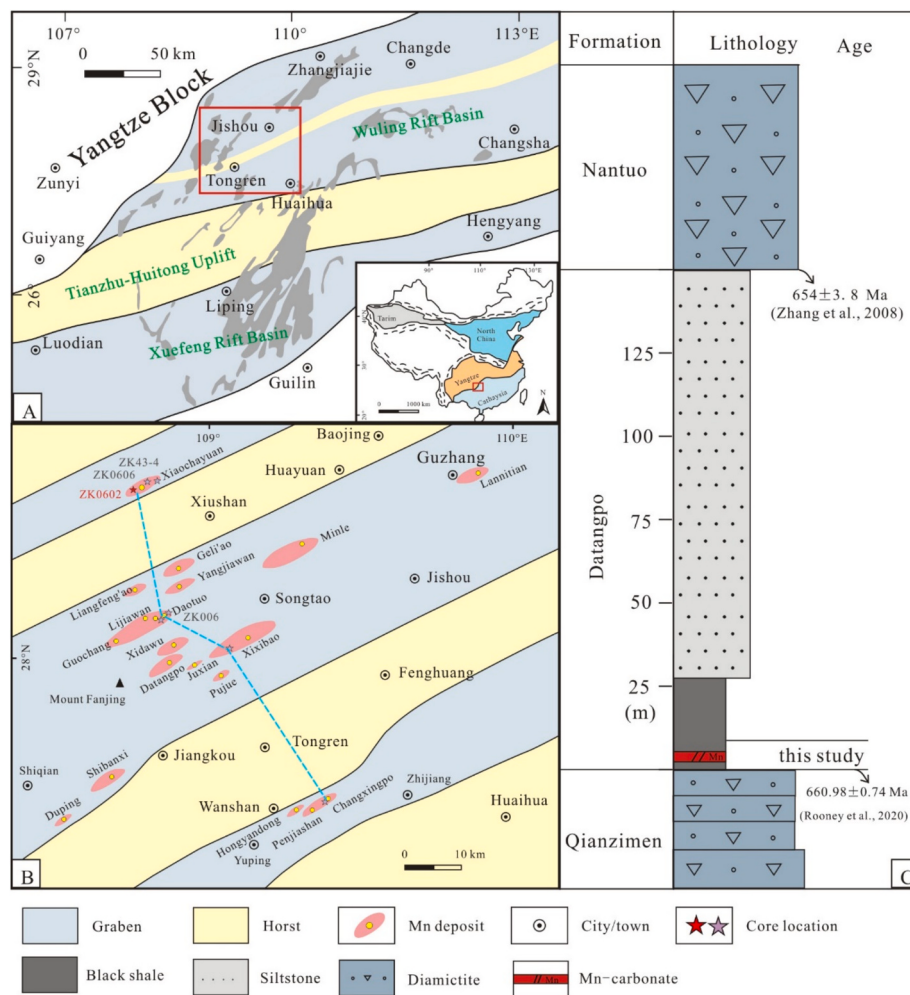


**Fig. 1.** Geological framework of the investigated Cryogenian Datangpo Formation in South China. (A) Structure of the Nanhua Rift Basin on the southeast margin of the Yangtze Block (Zhou et al., 2016). (B) Tectonic structure and deposition distribution of manganese ore deposits in the Chongqing-Guizhou-Hunan adjacent area with study sections (Zhou et al., 2022). (C) Stratigraphic section of the Datangpo Formation from Core ZK0602, Xiushan, Chongqing.

with the intervening Tianzhu–Huitong uplift. The Wuling secondary rift basin is characterized by a series of NE–SW-trending subordinate grabens and horsts (Zhou et al., 2016; Zhou et al., 2022), and a number of manganese deposits have precipitated in the small grabens of the rift basin following a similar spreading direction (Fig. 1B).

Neoproterozoic stratigraphic successions in South China are well-exposed and comprise glacial and interglacial deposits. Two major glacial intervals have been identified in the basin: the older Qianzimen (Tiesiao/Chang'an/Gucheng) Formation is predominantly composed of diamictites and sandstones (Fig. 2A), corresponding to the Sturtian glaciation; the younger Nantuo Formation comprises diamictite, sandstone, and siltstone, corresponding to the Marinoan glaciation (Li et al., 2012; Yan et al., 2020). The interglacial Datangpo Formation between them is subdivided into two members: Member 1 consists of massive black shale interbedded with manganese ore (rhodochrosite), while Member 2, which is significantly thicker than Member 1, comprises grey mudstones and siltstones (Li et al., 2012). A zircon CA-ID-TIMS U–Pb age of  $660.98 \pm 0.74$  was reported from a tuffaceous layer at the base of the Datangpo Formation at Gaozeng (Rooney et al., 2020). Another tuffaceous layer situated immediately beneath the Marinoan Nantuo Formation at Maopingdong recorded an LA-ICP-MS U–Pb age of  $654.5 \pm 3.8$  Ma (Zhang et al., 2008). These ages provide constraints on the

timing of this interglacial interval (Fig. 1C). Cyclostratigraphic analysis reveals the Datangpo Formation persisted for 9.8 myr, spanning from 660 Ma to 650 Ma (Bao et al., 2018).

The drill core ZK0602 is situated in a small graben facies, in the northern part of Nanhua Basin, which is relatively shallower than the Daotuo, Xixibao, Gaodi and Minle sections in the southern part of Nanhua Basin (Fig. 1B). In this study area, the Datangpo Formation is subdivided into three lithological units: (1) a basal layer of black shales interbedded with manganese ore (ca. 5 m thick), (2) a lower section of black shale (ca. 20 m thick), and (3) an upper section of grey mudstone and siltstone (ca. 126 m thick). Our research focused on the basal black shale interbedded with manganese ore of the Datangpo Formation (Fig. 1C), as manganese mineralization is predominantly concentrated in this unit.

### 3. Samples and methods

Geochemical analysis was conducted on nine samples collected from the lower portion of the Datangpo Formation. For each sample, ~200 g of fresh samples were ground to a 200-mesh powder using an automated agate mill.

Geochemical analyses of different iron species—including pyrite-

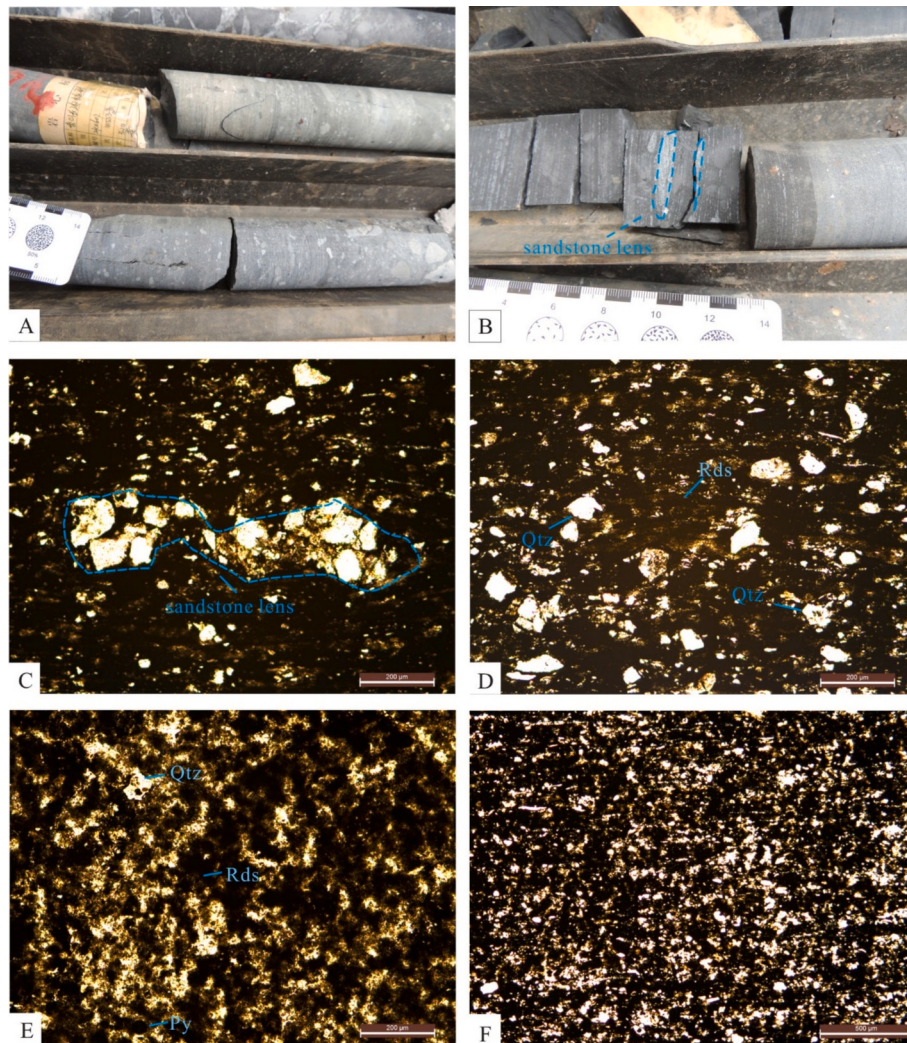


**Fig. 2.** Petrographic features of manganese-ore-bearing rocks from Core ZK0602.  
A. Diamictites and sandstone of the Qianzimen Formation; B. Carbonaceous mudstone intercalated with sandstone lenses; C. Carbonaceous mudstone intercalated with sandstone lenses; D. Carbonaceous mudstone containing rhodochrosite and quartz; E. Rhodochrosite associated with quartz and pyrite; F. Silty mudstone. Rds—rhodochrosite; Qtz—quartz; Py—pyrite.

bound iron ( $\text{Fe}_{\text{py}}$ ), oxide-bound iron ( $\text{Fe}_{\text{ox}}$ ), magnetite-bound iron ( $\text{Fe}_{\text{mag}}$ ), carbonate-associated iron ( $\text{Fe}_{\text{carb}}$ ), and highly reactive iron ( $\text{Fe}_{\text{HR}}$ )—along with the sulfur isotopic composition of pyrite ( $\delta^{34}\text{S}_{\text{py}}$ ), were performed at the State Key Laboratory of Biogeology and Environmental Geology, China University of Geosciences (Wuhan).  $\text{Fe}_{\text{py}}$  was stoichiometrically derived from the weight percentage of pyrite sulfur, which was extracted as an  $\text{Ag}_2\text{S}$  precipitate using the Cr-reduction method (Canfield et al., 1986).  $\text{Fe}_{\text{ox}}$ ,  $\text{Fe}_{\text{mag}}$ , and  $\text{Fe}_{\text{carb}}$  were quantified via a sequential extraction procedure as described by (Poulton and Canfield, 2005). For  $\delta^{34}\text{S}_{\text{py}}$  analysis,  $\text{Ag}_2\text{S}$  precipitates from the Cr-reduction step were combined with excess  $\text{V}_2\text{O}_5$  and measured using a Thermo Scientific Delta V Plus isotope ratio mass spectrometer coupled to a Flash elemental analyzer (Jin et al., 2016). Total organic carbon (TOC) was calculated as the difference between total carbon (TC) and total inorganic carbon (TIC). TC was determined by online combustion at 1350 °C using a Jena multi-EA 4000 carbon–sulfur analyzer, while TIC was measured via acidification with 30–40 % phosphoric acid.

Major and trace element analyses were carried out at the Southwestern Center of Experimentation, Ministry of Natural Resources. For major elements—including total iron content ( $\text{Fe}_T$ ) and aluminum (Al) content—analysis was performed using X-ray fluorescence (XRF) with an analytical accuracy of <1 %. Trace elements were extracted from dried bulk powders via  $\text{HF}/\text{HNO}_3/\text{HClO}_4$  digestion and quantified by inductively coupled plasma mass spectrometry (ICP-MS), achieving an analytical accuracy of <5 %.

The chemical index of alteration (CIA), a traditional proxy for chemical weathering intensity, is calculated using the molecular proportion:  $\text{CIA} = 100 \times [\text{Al}_2\text{O}_3/(\text{Al}_2\text{O}_3 + \text{CaO}^* + \text{Na}_2\text{O} + \text{K}_2\text{O})]$ . Here,  $\text{CaO}^*$  denotes the CaO content in the silicate fraction of the rock (Nesbitt and Young, 1982).

The enrichment factors of certain elements (e.g.,  $\text{Mo}_{\text{EF}}$ ) were calculated using the following formula:  $\text{X}_{\text{EF}} = [(\text{X}/\text{Al})_{\text{sample}}/(\text{X}/\text{Al})_{\text{PAAS}}]$ , where X and Al denote the weight concentrations of the elements X and Al. Samples were normalized against the post-Archean average shales (PAAS) as defined by Taylor and McLennan (1985). Enrichment factor values >1 indicate enrichment relative to PAAS. Specially,  $\text{X}_{\text{EF}} > 3$  signifies detectable enrichment, while  $\text{X}_{\text{EF}} > 10$  imply substantial enrichment (Algeo and Tribouillard, 2009). The results are interpreted using principles outlined in Algeo and Tribouillard (2009) and Algeo and Rowe (2012).

## 4. Results

### 4.1. Petrographic observations

The basal strata of the Datangpo Formation are predominantly composed of black mudstone, which can be subdivided into three distinct lithological units from base to top. The lower unit consists of carbonaceous mudstone interspersed with sandstone lens or bands (Fig. 2B, C), reflecting fine-grained deposition caused by the rapid rise in sea level following the termination of the Sturtian glaciation. The sandstone lens may represent glacial residual deposits. The overlying unit comprises carbonaceous mudstone with minor quartz grains, interbedded with rhodochrosite bands or lens (Fig. 2D). Pyrite is present in both the carbonaceous mudstone and rhodochrosite samples, occurring as frambooids or disseminated euhedral grains (Fig. 2E). Amorphous organic matter in the manganese ore samples is typically distributed along the margins of the rhodochrosite crystals. These sedimentary features indicate sea-level rise due to deglaciation, while the presence of rhodochrosite may suggest a decline in sea level during transient glacial stadials. The upper unit is composed of silty mudstone, with an increased proportion of detrital minerals (e.g., quartz, feldspar) compared to the underlying carbonaceous mudstone. The abundance of organic matter-rich components decreases from the lower to the upper units (Fig. 2F), implying a slight decline in sea level.

### 4.2. Geochemical characteristics

The geochemical characteristics of samples from the basal Datangpo Formation in core ZK0602—including iron speciation, concentrations of redox-sensitive trace elements (Mo, U, and V), Sr, Ba, Ca, Mn, TOC, CIA, and  $\delta^{34}\text{S}_{\text{py}}$ —are summarized in Table 1, with their stratigraphic variations illustrated in Fig. 3. Based on the stratigraphic succession and associated geochemical characteristics, the basal Datangpo Formation is subdivided into four distinct intervals (Fig. 3).

Interval I is marked by black shales that exhibit high  $\text{Fe}_{\text{HR}}/\text{Fe}_T$  (> 0.5) and  $\text{Fe}_{\text{py}}/\text{Fe}_{\text{HR}}$  (> 0.8), along with moderate to high TOC content (4.96 %). The concentrations of Mo, U, V, Al and  $\delta^{34}\text{S}_{\text{py}}$  are 36.0 ppm, 2.91 ppm, 128 ppm, 8.2 %, and 36.42 %; however, the content of Mn and Sr/Ba are only 0.19 % and 0.11.

Interval II is distinguished by black shales intercalated with Mn-carbonate, which corresponds to the layers of manganese ore in the studied area. This interval exhibits variable ratios of  $\text{Fe}_{\text{HR}}/\text{Fe}_T$  (0.61–0.83),  $\text{Fe}_{\text{py}}/\text{Fe}_{\text{HR}}$  (0.02–0.48), and low TOC content (1.58 % – 2.40 %). The concentrations of Mo, U, V, Al and  $\delta^{34}\text{S}_{\text{py}}$  are 1.52 ppm – 3.7 ppm, 0.88 ppm – 1.34 ppm, 64.4 ppm – 82.0 ppm, 2.06 % – 2.10 %, and 47.12 % – 52.06 %, respectively. Notably, the Mn value ranges from 20.49 % to 21.28 %, and the Sr/Ba ranges from 1.08 to 1.14, representing a significant increase compared to interval I.

Interval III corresponds to black shales, characterized by relatively high  $\text{Fe}_{\text{HR}}/\text{Fe}_T$  (0.59–0.86) and  $\text{Fe}_{\text{py}}/\text{Fe}_{\text{HR}}$  (0.89–0.94). Additionally, this interval exhibits a high TOC content (3.78 % – 5.43 %), as well as elevated concentrations of Mo (31.8 ppm – 50.0 ppm), U (3.12 ppm – 3.78 ppm), V (123.0 ppm – 199.0 ppm), Al (8.12 % – 11.53 %), and  $\delta^{34}\text{S}_{\text{py}}$  (43.55 % – 55.17 %), respectively. In contrast, the Mn content and Sr/Ba decrease to a range of 0.15 % – 0.67 % and 0.07–0.10.

Interval IV is marked by black shales containing a small amount of silt, exhibiting high  $\text{Fe}_{\text{HR}}/\text{Fe}_T$  (0.06–0.99) and  $\text{Fe}_{\text{py}}/\text{Fe}_{\text{HR}}$  (0.92–0.93). The TOC content deceases compared to interval III, ranging from 2.71 % to 4.2 %. The Mo content decreases, ranging from 12.5 ppm to 28.0 ppm, while the U, V, Al and  $\delta^{34}\text{S}_{\text{py}}$  content show slight decreases compared to interval III, falling within the ranges of 3.21 ppm – 3.42 ppm, 114.0 ppm – 162.0 ppm, 8.59 % – 9.39 %, and 49.74 % – 54.61 %, respectively. The Mn value range between 0.17 % and 0.89 %, and the Sr/Ba range between 0.08 and 0.11, which are comparable to those found in intervals I and III.

## 5. Discussions

### 5.1. Bottom water redox condition of the basal Datangpo Formation at ZK0602

Iron speciation, redox-sensitive trace elements and TOC are widely recognized as robust indicators of paleoredox conditions (Canfield et al., 2008; Algeo and Tribouillard, 2009; Li et al., 2012). According to established geochemical criteria (Poulton and Canfield, 2011), a combination of  $\text{Fe}_{\text{HR}}/\text{Fe}_T > 0.38$  and  $\text{Fe}_{\text{py}}/\text{Fe}_{\text{HR}}$  ratio > 0.8 signifies euxinic bottom-water environments, whereas  $\text{Fe}_{\text{HR}}/\text{Fe}_T > 0.38$  coupled with  $\text{Fe}_{\text{py}}/\text{Fe}_{\text{HR}} < 0.8$  may suggest anoxic but sulfide-free (ferruginous) conditions. A critical constraint from Clarkson et al. (2014) highlights that  $\text{Fe}_T > 0.5$  % serves as a minimum threshold for validating iron-based redox proxies in iron-poor, carbonate-dominated sediments. For redox-sensitive trace elements (e.g., Mo, U, and V), their higher solubility under oxic conditions and tendency to precipitate anoxic settings enable their use as proxies for redox fluctuations. Sedimentary concentrations of these elements have been widely applied to quantify the intensity of reducing conditions (Tribouillard et al., 2006; Algeo and Tribouillard, 2009).

Based on sedimentary characteristics and various geochemical proxies, four distinct intervals can be identified in the basal Datangpo Formation at ZK0602 (Fig. 3). In interval I, elevated concentrations of trace metals (Mo, U, and V) are consistent with iron speciation ratios

**Table 1**  
Geochemical data of the samples from the basal I Datangpo Formation at ZK0602.

Interval	Sample	depth (m)	$\text{Fe}_{\text{Py}}$ (%)	$\text{Fe}_{\text{HR}}$ (%)	$\text{Fe}_{\text{T}}$ (%)	$\text{Fe}_{\text{Py}}/\text{Fe}_{\text{HR}}$	$\text{Fe}_{\text{Py}}/\text{Fe}_{\text{T}}$	TOC (%)	$\delta^{34}\text{S}_{\text{Py}}$ (‰)	Mo (ppm)	U (ppm)	V (ppm)	Al (%)	CIA (%)	Mn (%)	CaO (%)	Sr (ppm)	Ba (ppm)
I	H1	0.2	1.60	1.86	3.51	0.53	0.86	0.43	4.96	36.42	2.91	128	8.20	74.09	0.19	1.33	111	1010
	H2	0.8	0.03	1.38	2.27	0.61	0.02	1.10	2.40	47.12	1.52	0.88	64.4	2.06	69.92	21.28	9.46	352
	H3	1.4	0.87	1.81	2.20	0.83	0.48	1.05	1.58	52.06	3.70	1.34	82	2.10	77.97	20.49	13.38	392
II	H4	2.0	2.95	3.15	3.66	0.86	0.94	0.32	3.78	55.17	33.60	3.78	123	11.53	89.10	0.67	1.59	125
	H5	2.6	1.71	1.93	3.26	0.59	0.89	0.39	5.43	43.55	50.00	3.44	199	8.38	79.70	0.15	0.48	93
	H6	3.2	2.09	2.31	3.32	0.70	0.91	0.41	5.05	44.28	31.80	3.12	158	8.12	79.75	0.15	0.45	98.5
III	H7	3.8	/	0.23	3.94	0.06	/	0.46	4.20	/	12.50	3.21	114	8.65	82.15	0.17	0.44	97.1
	H8	4.4	2.19	2.38	3.26	0.73	0.92	0.35	2.71	54.61	25.00	3.28	162	9.39	81.94	0.22	0.46	99.4
	H9	5.0	4.37	4.67	4.73	0.99	0.93	0.55	3.76	49.74	28.00	3.42	160	8.59	84.16	0.89	0.68	961
IV																		104
																		986

speciation characteristics ( $\text{Fe}_{\text{HR}}/\text{Fe}_{\text{T}} > 0.38$  and the  $\text{Fe}_{\text{Py}}/\text{Fe}_{\text{HR}} > 0.8$ ), collectively indicating prevailing euxinic (sulfidic anoxic) bottom-water conditions. In interval II, a significant decline in trace metal (Mo, U, and V) concentrations suggests suboxic conditions. However, the combination of  $\text{Fe}_{\text{HR}}/\text{Fe}_{\text{T}} > 0.38$  and the  $\text{Fe}_{\text{Py}}/\text{Fe}_{\text{HR}} < 0.8$  denotes anoxic but sulfide-free (ferruginous) bottom waters. Integrating these parameters, Interval II is interpreted as a ferruginous environment. In interval III, Trace metal (Mo, U, and V) concentrations increase substantially, reaching peak values, which correlate with iron speciation ratios indicative of a return to euxinic conditions. By interval IV, Mo concentrations decline markedly, while U and V show slight decreases or stability relative to Interval III. With  $\text{Fe}_{\text{HR}}/\text{Fe}_{\text{T}} > 0.38$  and  $\text{Fe}_{\text{Py}}/\text{Fe}_{\text{HR}} > 0.8$ , this interval suggests moderately euxinic conditions.

A robust positive correlation between  $\text{Fe}_{\text{Py}}$  and  $\text{Fe}_{\text{HR}}$  is evident (Fig. 4A), demonstrating that these black shales of basal Datangpo Formation were predominantly deposited under euxinic bottom waters conditions characterized by iron limitation (Li et al., 2012). Additionally, stratigraphic records spanning the Paleoproterozoic to Neoproterozoic exhibit a broad distribution in  $\text{Fe}_{\text{Py}}/\text{Fe}_{\text{HR}}$  versus  $\text{Fe}_{\text{HR}}/\text{Fe}_{\text{T}}$  crossplot. This geochemical pattern aligns with the coexistence of sulfidic waters along ocean margins or within restricted basins and a ferruginous deep oceanic environment (Planavsky et al., 2011; Li et al., 2012; Ma et al., 2019). Data from ZK0602 samples show that the restricted interglacial Nanhua Basin was dominated by euxinic conditions during deposition of the lower Datangpo Formation, with intermittent ferruginous intervals that facilitated rhodochrosite precipitation (Fig. 3, Fig. 4B).

In the  $\text{Mo}_{\text{EF}}$  vs.  $\text{U}_{\text{EF}}$  diagram, the sample distributions indicate that intervals I, III, and IV were predominantly deposited under euxinic conditions. Notably, two rhodochrosite samples from interval II plot within the ferruginous zone, implying weaker reducing conditions compared to the other three intervals of the Datangpo Formation (Fig. 5). A striking observation is the significant enrichment of Mo (EFs: 6.18–50.12) relative to U (EFs: 3.03–5.9) (Fig. 5). Previous studies attributed the covariation between  $\text{Mo}_{\text{EF}}$  and  $\text{U}_{\text{EF}}$  to the Mn–Fe particulate shuttle mechanism, which is linked to Mn–Fe redox cycling (Algeo and Tribouillard, 2009). Others researchers proposed that the preferential enrichment of Mo over U may reflect the coexistence of a moderately enriched oceanic Mo reservoir and a depleted U reservoir (Ye et al., 2018).

## 5.2. Bottom water redox state fluctuation and openness of the Nanhua Basin

### 5.2.1. Bottom water redox state fluctuation of the Nanhua Basin

During the early Cryogenian interglacial period, anoxic (predominantly euxinic) conditions generally prevailed, interrupted by intermittent ferruginous intervals. This perspective is supported by iron speciation and redox-sensitive trace elements (Mo, U, and V) data from the lower Datangpo Formation at the ZK0602 in the Chongqing area (Figs. 3, 7). Analogous redox fluctuations have been documented at the Minle section (Hunan Province), Daotuo section (Guizhou Province), and ZK43–6 core (Chongqing City) (Figs. 6, 7) (Li et al., 2012; Zhang et al., 2015; Cheng et al., 2018; Ma et al., 2019; Wu et al., 2024). These observations collectively suggest a regional-scale pattern of alternating euxinic and ferruginous conditions in the basal Datangpo Formation (Fig. 7). The size distribution of pyrite framboids in the basal Datangpo Formation black shales—characterized by a mean diameter of ~5 µm and narrow standard deviation (within ±2 µm)—also likely reflects euxinic bottom-water conditions (Ye et al., 2018; Zhu et al., 2022). However, the restricted tectonic setting of the Nanhua Basin (Wang and Li, 2003; Li et al., 2012) may limit the extrapolation of these redox signatures to open oceanic environments.

The black shales and manganese ores from core ZK0602 at Xiushan, Chongqing, exhibit exceptionally heavy  $\delta^{34}\text{S}_{\text{Py}}$ , ranging from 36.42 to 55.17 ‰ (Table 1). Similarly enriched  $\delta^{34}\text{S}_{\text{Py}}$  values have been reported

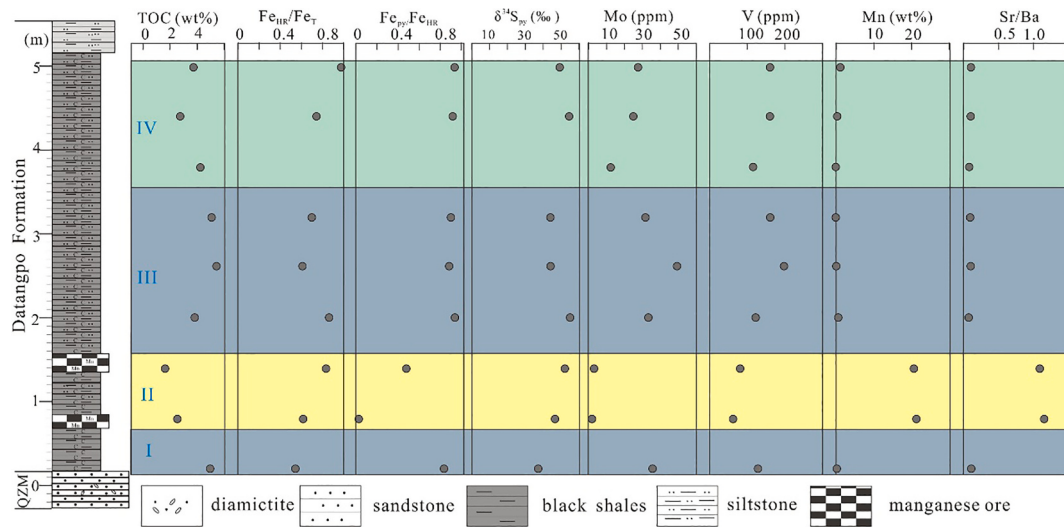


**Fig. 3.** Composite chemostratigraphy with TOC, iron speciation,  $\delta^{34}\text{S}_{\text{py}}$ , Mo, V, Mn, and Sr/Ba from the basal Datangpo Formation at ZK0602. Intervals (I to IV) are defined by the lithology and geochemical characteristic (TOC, Mn, Mo, V, Sr/Ba, and iron speciation) described in the text. QZM, Qianzimen Formation.

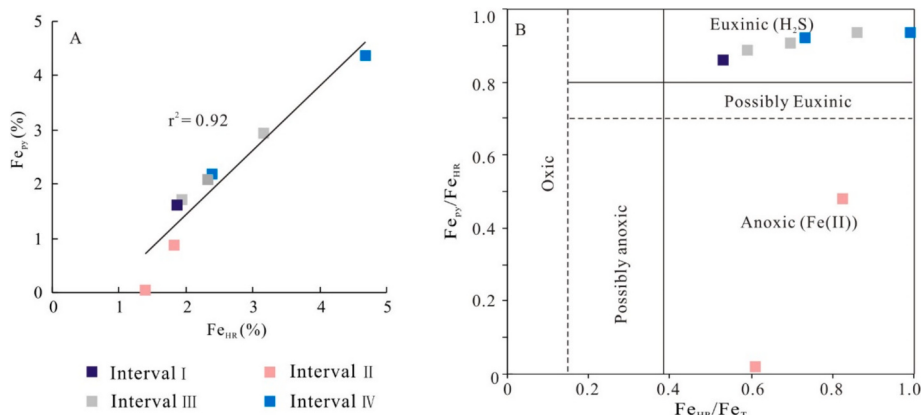


**Fig. 4.** Crossplots of  $\text{Fe}_{\text{py}}$  versus  $\text{Fe}_{\text{HR}}$  (A) and  $\text{Fe}_{\text{py}}/\text{Fe}_{\text{HR}}$  versus  $\text{Fe}_{\text{HR}}/\text{Fe}_T$  (B) for samples from the basal Datangpo Formation in Core ZK0602. Solid and dashed lines in crossplots (B) denote redox boundaries of the water column. The lower boundary value of  $\text{Fe}_{\text{HR}}/\text{Fe}_T$  ( $0.15 \pm 0.1$ ) might be applicable for mature samples, such as those from the Datangpo Formation (Raiswell et al., 2008).

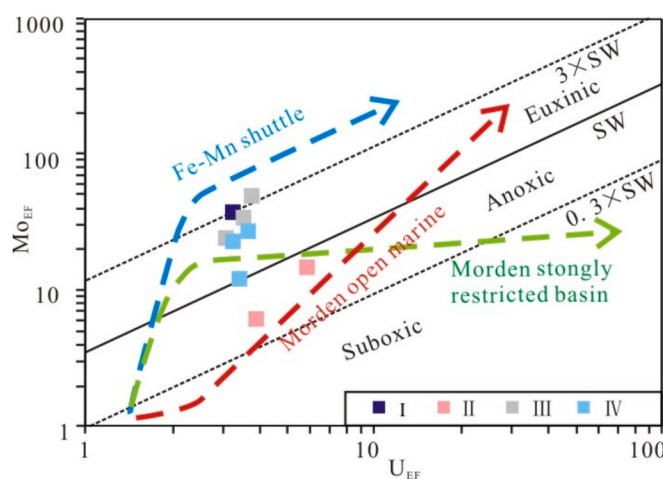


**Fig. 5.** Crossplots of  $\text{Mo}_{\text{EF}}$  versus  $\text{U}_{\text{EF}}$  from the basal Datangpo Formation in Core ZK0602. The solid and dashed lines are modified from Algeo and Tröbärg (2009).

from contemporaneous Cryogenian successions across South China, including the Xiangmeng, Zhalanggou, Tanganshan, Xiadawu, Changxingpo, Penjiasha, Hongyandong, and Minle sections (Fig. 8, Table 2) (Li et al., 1999; Chu et al., 2003; Liu et al., 2006; Chen et al., 2008; Feng et al., 2010; Li et al., 2012; Wang et al., 2016; Ma et al., 2019; Liu et al., 2021a; Cai et al., 2022).

Such heavy  $\delta^{34}\text{S}_{\text{py}}$  values are generally interpreted as the result of a limited marine sulfate reservoir, which enhances Rayleigh-type isotopic fractionation during microbial sulfate reduction (MSR) (Canfield, 2001; Fike et al., 2015). In addition, other environmental and diagenetic processes—such anaerobic oxidation of methane (Jørgensen et al., 2004) and rapid sedimentation rates (Liu et al., 2019)—can contribute to the formation of  $^{34}\text{S}$ -enriched pyrite. Although thermochemical sulfate reduction (TSR) during late-stage burial has been proposed as a potential mechanism for generating such high  $\delta^{34}\text{S}_{\text{py}}$  values in the Datangpo Formation (Cui et al., 2018), the spatially widespread occurrence of these isotopic signatures across multiple sections suggests that they primarily reflect contemporaneous seawater sulfate concentrations rather than localized diagenetic overprints or depositional controls.

Through Earth's history, sulfate concentrations have exhibited a gradual increase (Anbar and Knoll, 2002; Kah et al., 2004). However, evidence suggests that the Cryogenian ocean may have harbored low sulfate concentrations, implying significant changes in sulfur cycling

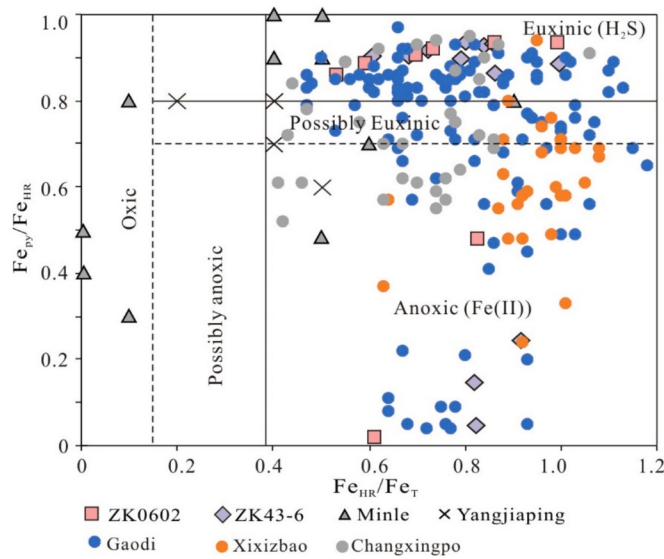


**Fig. 6.** Crossplots of  $\text{Fe}_{\text{py}}$  versus  $\text{Fe}_{\text{HR}}$  and  $\text{Fe}_{\text{py}}/\text{Fe}_{\text{HR}}$  versus  $\text{Fe}_{\text{HR}}/\text{Fe}_T$  for the samples from the Datangpo Formation of the Nanhua Basin. Sources: Minle is from Li et al. (2012); Yangjiaping is from Li et al. (2012); ZK43-6 is from Ma et al. (2019); Gaodi, Xixibao and Changxingpo are from Cheng et al. (2021). The Solid and dashed lines denote the water column redox boundaries (modified from Raiswell et al., 2008 and Li et al., 2012).

during this period. During the Sturtian and Marinoan glaciations, the hydrologic cycle was suppressed, likely reducing the riverine flux of sulfate to the ocean (Hoffman et al., 1998; Hoffman et al., 2017). Concurrently, under the extensive sea ice cover of the Sturtian glaciation, the development of ocean anoxia would have facilitated the removal of marine sulfate via microbial sulfate reduction. During the Sturtian glaciation, sea-level decline likely fostered the development of numerous semi-restricted sub-basins within the Nanhua Basin (Li et al., 1999; Wang and Li, 2003). Compared to coeval open-ocean environments, these sub-basins would have exhibited lower sulfate concentrations and elevated  $\delta^{34}\text{S}_{\text{py}}$  values (Chen et al., 2008; Cai et al., 2022). Post-Sturtian glaciation, enhanced continental weathering and

increased riverine sulfate flux to the ocean should have raised marine sulfate levels. However, the sulfate reservoir may have remained limited due to the persistently low background sulfate concentrations established during the Sturtian glaciation (Feng et al., 2010). The formation of super-heavy  $\delta^{34}\text{S}_{\text{py}}$  values immediately after the Sturtian Snowball Earth has been attributed to a two-stage mechanism involving microbial sulfate reduction in meltwater-influenced, sulfate-depleted settings followed by early diagenetic reactions with  $^{34}\text{S}$ -enriched sulfate from overlying euxinic or ferruginous seawater (Cai et al., 2022). We therefore interpret the heavy  $\delta^{34}\text{S}_{\text{py}}$  values in the Datangpo black shales as a robust proxy for a sulfate-depleted ocean during the Cryogenian interglacial, characterized by pervasive microbial sulfate reduction within a restricted rift basin in South China (Jørgensen et al., 2004; Feng et al., 2010; Li et al., 2012; Liu et al., 2019).

### 5.2.2. Openness of the Nanhua Basin

Fluctuations in bottom-water redox states may correlate with changes in the Nanhua Basin's openness to the open ocean. The relationship between Mo and TOC contents could offer insights into the degree of restriction of the subchemoclinal water mass. As the connectivity between sedimentary basins and the open ocean influences supply and burial of Mo, modern sediments deposited under similar anoxic conditions exhibit higher Mo contents in more connected basins than in more restricted basins (Algeo and Lyons, 2006; Algeo and Rowe, 2012). Additionally, because sedimentary Mo typically accumulates in organic-rich marine sediments deposited under anoxic conditions (Algeo and Lyons, 2006; Algeo and Rowe, 2012), the combined use of Mo and TOC can effectively characterize the degree of restriction in marine systems.

Plotting the Mo and TOC data of the black shales and manganese ore layers of the basal Datangpo Formation in Nanhua Basin reveals that most data points fall within the region of  $\text{Mo}/\text{TOC} < 9$ , indicating relatively restricted basin environments. Further comparative analysis shows that the data from ZK0602, ZK43-6, Yangjiaping, Changxingpo, and Minle section are distributed in the region with  $\text{Mo}/\text{TOC}$  values between 4.5 and 9, while the data from Xixibao and Gaodi sections fall into the region with  $\text{Mo}/\text{TOC} < 4.5$  (Fig. 9). This demonstrates that the latter deposited in more restricted conditions, which is consistent with their paleogeographical positions in the center of the Nanhua Rift Basin (Wang and Li, 2003; Zhou et al., 2022).

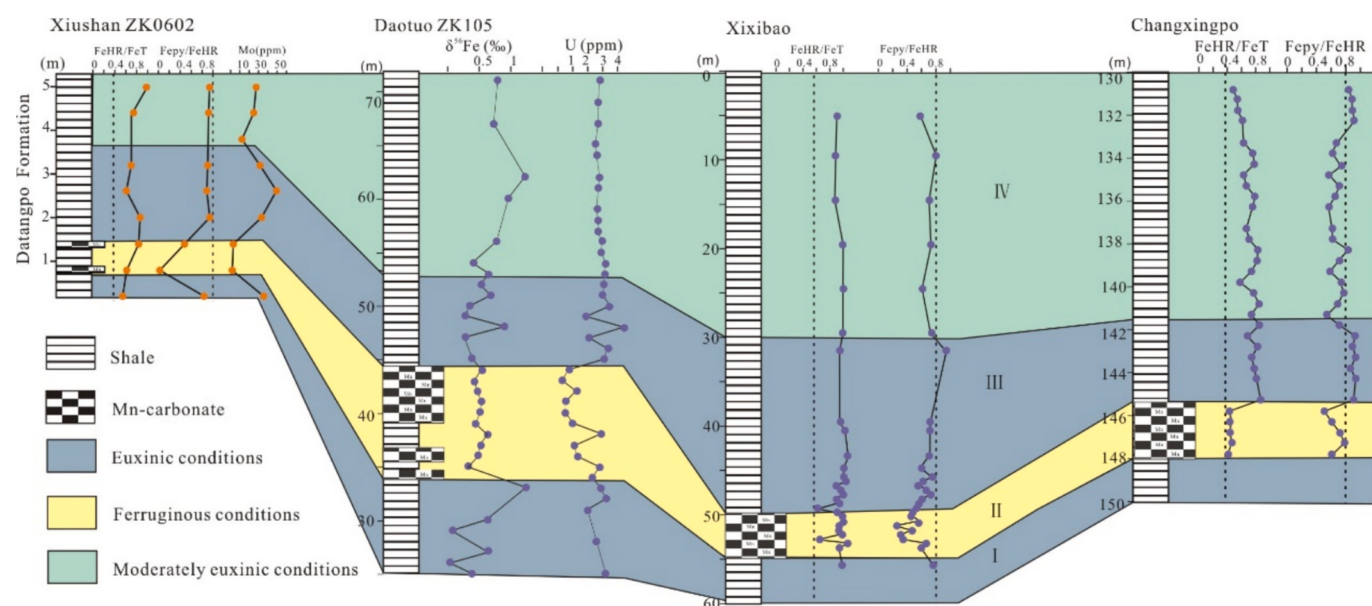


**Fig. 7.** Comparison of redox conditions in the basal Datangpo Formation across studied sections.

Xixibao and Changxingpo sections are from Cheng et al. (2021); ZK105 at Daotuo is from Zhang et al. (2015); ZK0602 is from this study. The above-mentioned sections and drill cores are positioned in Fig. 1.

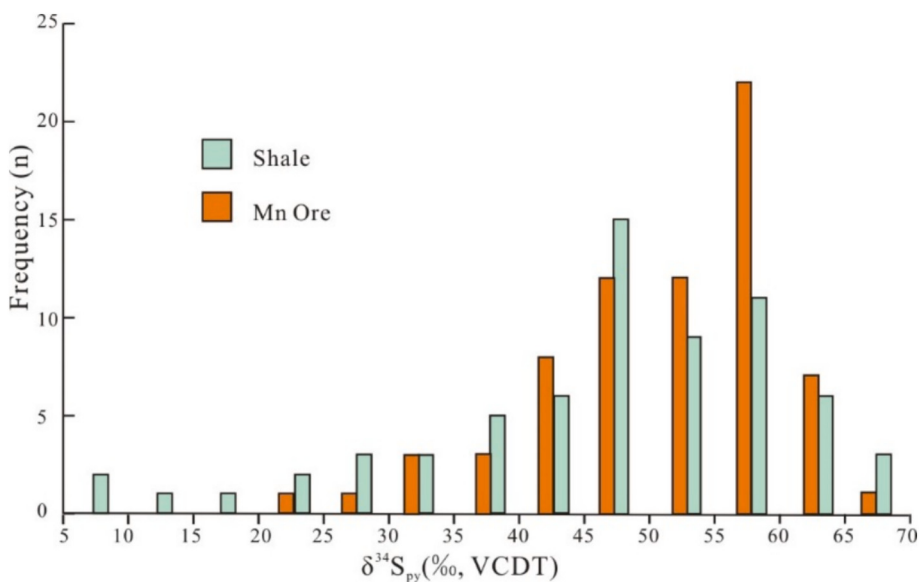


**Fig. 8.** Frequency distribution of  $\delta^{34}\text{S}_{\text{py}}$  from the Datangpo Formation in the Nanhua Basin.

Data are from Li et al. (1999), Chu et al. (2003), Liu et al. (2006), Chen et al. (2008), Feng et al. (2010), Li et al. (2012), Wang et al. (2016), Ma et al. (2019), Cai et al. (2022) and this study.

**Table 2**  
Summary of  $\delta^{34}\text{S}_{\text{py}}$  of the lower black shales and Mn ore of the Datangpo Formation.

Section	depth	Sample number	Range (‰)	Mean (‰)	Reference
Tianping	Shallow	5	21.10–35.70	27.0	Chu et al. (2003)
Xiangtan	Shallow	15	15.36–63.80	47.56	Li et al. (1999); Liu et al. (2006)
Yangjiaping	Shallow	15	5.60–37.50	20.05	Chu et al. (2003); Li et al. (2012)
Tanganshan	Shallow	6	23.78–31.41	29.34	Liu et al. (2006)
Xiushan	Deep	24	21.30–56.79	45.96	Li et al. (1999); Ma et al. (2019); this study
Xiadawu	Deep	7	30.5–51.3	44.26	Cai et al. (2022)
Songtao	Deep	28	36.80–66.76	56.44	Li et al. (1999); Wang et al. (2016)
Zhailanggou	Deep	6	31.70–59.40	50.55	Chen et al. (2008)
Minle	Deep	37	16.1–69.0	52.44	Feng et al. (2010); Li et al. (1999); Li et al. (2012)
Changxingpo	Deep	6	37.5–58.4	49.95	Cai et al. (2022)
Penjishan	Deep	2	33.2–50.7	41.95	Cai et al. (2022)
Hongyandong	Deep	4	37.3–57.5	46.03	Cai et al. (2022)

### 5.3. Paleosalinity variations of the basal Datangpo Formation in Nanhua Basin

Despite the Cryogenian Nanhua Basin's long-standing interpretation as a fully marine basin (Wang and Li, 2003), secular fluctuations in its water mass salinity are plausible given its paleogeographic environments. Specifically, the connectivity of this semi-restricted basin to the open ocean would have been influenced by eustatic variations, tectonic movements, and climatic shifts. In this study, we utilized Sr/Ba ratios,

integrated with B/Ga data from previous studied sections to assess salinity changes of the basal Datangpo Formation in Nanhua Basin. B/Ga ratios  $>6.0$  and Sr/Ba ratios  $>0.5$  are diagnostic of marine water conditions, whereas values  $<3.0$  for B/Ga or  $<0.2$  for Sr/Ba indicate freshwater deposition. Intermediate ratios serve as proxies for brackish or mixed-water environments (Wei and Algeo, 2020; Liu et al., 2021b).

All black shale samples exhibit lower Sr/Ba ratios ( $<0.2$ ), indicative of fresh-water conditions, while the manganese ore layers record significantly higher values (1.08–1.14), reflecting marine conditions (Fig. 3). Previous studies have indicated that the incorporation of carbonate-hosted Sr can significantly elevate bulk-rock Sr/Ba ratios, thereby undermining the reliability of using Sr/Ba ratios to evaluate salinity conditions (Wei and Algeo, 2020). In this study, ZK0602 show low carbonate (shown as CaO) contents (0.44 % to 13.38 %, mean = 3.14 %), but for samples in interval II show high carbonate (shown as CaO) contents (9.46 % to 13.38 %, mean = 11.42 %). Thus, it is necessary to further examine the potential influence of carbonate-hosted Sr on our Sr/Ba proxy. As shown in (Fig. s1A), almost all samples display positive covariance of Sr/Ba values and CaO contents. After filtering samples with CaO content  $>2.3$  % (equal to 4 % CaCO<sub>3</sub>, e.g., Remírez and Algeo, 2020), seven samples also show positive covariance of Sr/Ba ratios and CaO contents (Fig. s1B). Therefore, it is reasonable to use Sr/Ba as a paleosalinity indicator in the intervals I, III and IV (CaO  $< 2.3$  %), while its use as a paleosalinity indicator in interval II (CaO  $> 2.3$  %) requires further verification.

By comparing with other studies in the Nanhua basin, it is found that drill cores from the Gaodi, Xixibao, Xiadawu and Changxingpo manganese ores exhibit similar variations of paleosalinity evidenced by Sr/Ba and B/Ga ratios (Fig. 10) (Cheng et al., 2021; Cai et al., 2022). The elevated Sr/Ba ratios in the manganese ore layers can be attributed to the carbonate-hosted Sr, a phenomenon driven by the similar ionic radii of Sr and Ca, which facilitate Sr incorporation into carbonate minerals. Although exceptionally high sedimentary Ba concentrations could theoretically arise from enhanced biological productivity or BaSO<sub>4</sub> precipitation (Paytan and Griffith, 2007), the study samples display Ba concentrations consistent with typical shales, and exhibit positive Ba—Al correlations (Fig. s1C), indicating no evidence of excess Ba. Conversely, the unusually low Sr concentrations observed are more likely the primary driver of low Sr/Ba ratios. Recent research highlights that Neoproterozoic and Cambrian strata systematically yield lower Sr/

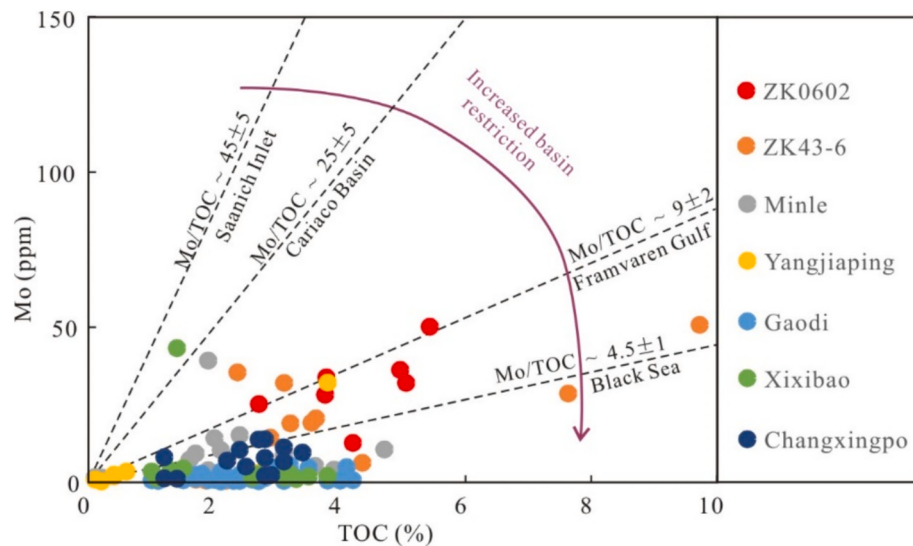


**Fig. 9.** Crossplots of sedimentary Mo versus TOC for samples from the basal Datangpo Formation. The regression lines are based on the work of Algeo and Lyons (2006). The cited data for the Minle Section and Yangjiaping section is from Li et al. (2012), the data for ZK43-6 at Chongqing is from Ma et al. (2019), and the data for Gaoxi, Xixibao and Changpingpo section is from Cheng et al. (2021).

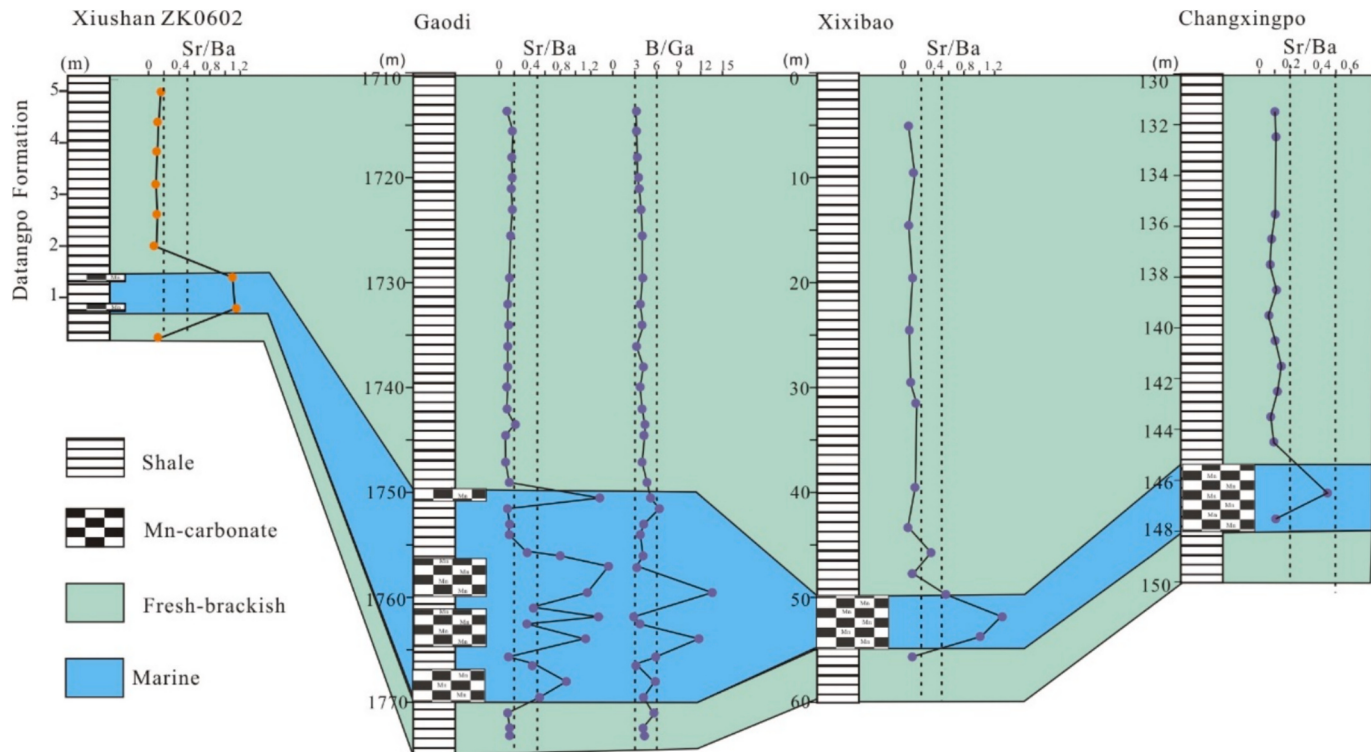


**Fig. 10.** Comparison of paleosalinity in the basal Datangpo Formation across studied sections.

Gaodi, Xixibao and Changxingpo sections are from Cheng et al. (2021); ZK0602 is from this study. The above-mentioned sections and drill cores are positioned in Fig. 1.

Ba ratios compared to younger units, potentially reflecting reduced Sr availability in the contemporary ocean. While B/Ga and S/TOC are generally regarded as more robust salinity proxies (Wei and Algeo, 2020), the Sr/Ba profile at the Gaodi manganese deposit in Guizhou Province closely resembles that of the B/Ga proxy (Cheng et al., 2021). The salinity fluctuations derived from the Sr/Ba data of ZK0602—that the black shale was formed in a brackish water environment and the manganese ore in a marine environment—is consistent with the understanding obtained from the B/Ga data of other sections (Cheng et al.,

2021; Wei et al., 2024).

The salinity of water mass in a marginal basin is governed by the overall water balance, involves the balance between precipitation/runoff and evaporation, as well as the extent of water exchange with the open ocean (Matthias and Godfrey, 1994). Modern open-ocean seawater has an average salinity of approximately 35 psu, in contrast to freshwater with salinities <1 psu. Increased freshwater inputs or diminished oceanic exchange can drive decreases in marginal-marine basin salinity, as evidenced by case studies in the Japan Sea and Mediterranean Sea.

During the Late Quaternary glacio-eustatic lowstands, both water bodies experienced pronounced salinity reductions due to substantial freshwater runoff into increasingly restricted basins (Keigwin and Gorbarenko, 1992). Tectonic sills along the margins of the Cryogenian Nanhua Rift Basin likely constrained water mass exchange with the open ocean, thereby creating conditions for secular fluctuations in water mass salinity.

Salinity proxies consistently reveal oscillations between fresh-brackish water conditions during black shale deposition and fully marine environments during manganese ore accumulation (Fig. 10). This depositional pattern implies that black shale intervals were modulated by either enhanced freshwater input or restricted incursion of open-ocean waters. Mercury isotope signatures corroborate greenhouse climate conditions (Zhou et al., 2021), while elevated CIA values and lithium isotope compositions document intense chemical weathering (Wang et al., 2020; Wei et al., 2020) during the black shales in the basal Datangpo Formation.

The index of CIA and Sr/Ba of the Datangpo Formation show a negative correlation in the Nanhua Rift Basin (Fig. 11A). This indicates that during the interglacial period, due to the increase in temperature, chemical weathering is enhanced and the terrestrial input increases, which may lead to a decrease in the salinity of the water column. However, during the glacier stadial within the interglacial period, the terrestrial input will decrease, thus causing the salinity of the water column to reach the salinity of seawater. This suggests that enhanced precipitation and runoff may have contributed to the reduction of basinal salinity. Meanwhile, the content of MnO shows a positive correlation with the salinity proxy Sr/Ba (Fig. 11B), which further reveals that a high-salinity seawater environment is conducive to the formation of manganese ore.

#### 5.4. A model for Datangpo manganese metallogenesis

##### 5.4.1. Origin of manganese

Positive Eu anomalies are typically regarded as evidence of hydrothermal activity (Peter, 1996). Notably, several occurrences of positive Eu anomalies in low-temperature settings have been documented, which are presumably linked to organic-rich sediments under sulfate-reducing conditions (Kidder et al., 2003). The significance of hydrogenous inputs as a source of manganese in the Datangpo Formation is supported by Eu/Eu\* ratios, which average 0.94 for the manganese ore samples, compared to approximately 0.8 for the hydrogenous endmember and around 1.5 for the hydrothermal endmember (Yu et al., 2016; Xiao et al., 2017). The manganese ore samples from ZK0602 exhibit a weak positive Eu anomaly, with an average Eu/Eu\* of 1.19. This suggests a mixture of hydrogenous and hydrothermal source endmembers, likely resulting from the reducing alkaline pore water environment (Xiao et al., 2017).

Negative Ce anomalies are generally regarded as a useful marker of hydrothermal activity, with a Ce/Ce\* value of approximately 0.46 in modern oceans (Hein et al., 1996). In contrast, strongly positive Ce anomalies may indicate a hydrogenous source (Usui and Someya, 1997;

Bau et al., 2014; Xiao et al., 2017). The Datangpo manganese deposits predominantly exhibit positive Ce anomalies, with an average value of 1.06 at for manganese ore samples from ZK0602, suggesting a primarily hydrogenous source of Mn.

Liu et al. (2006) suggested that the Mn in the Datangpo Formation may have been transported by glaciation, which scraped off tropical soils rich in Fe and Mn in the form of oxides. These soils were subsequently dumped into small, semi-restricted sub-basins with limited exchange with the open oceans.

Dobrzinski et al. (2004) utilized CIA to investigate the weathering intensity of source area for the Neoproterozoic sedimentary rocks in South China. Their findings showed that the lower Sturtian tillite had an average CIA value of 62, interglacial deposits exhibited a value of 71, and the upper Marinoan glacial tillite recorded 65. In interval II of ZK0602, the CIA values range from 69.9 to 89.1, with a mean of 79.89 (Fig. 11). In contrast, the CIA of modern glacial marine sediments in the Scotia Sea averages only 55 (Diekmann et al., 2000), while modern soils have an average CIA of 72 (Maynard, 1992). Therefore, the weathering intensity of the source area of the Datangpo Formation indicates a higher degree of weathering compared to modern soils. A significantly negative  $\delta^7\text{Li}$  excursion of  $\sim -5\%$  has also been detected in the basal Datangpo Formation, indicating a substantial increase in chemical weathering intensity following the Sturtian glaciation (Wei et al., 2020). Concurrently, elevated Hg concentrations, high Hg/TOC ratios, and positive  $\Delta^{199}\text{Hg}$  in the basal Datangpo Formation point to extensive volcanic Hg emission at the initiation of the Cryogenian interglacial period (Zhou et al., 2021). Extensive volcanic activity not only emitted massive volumes of volcanic rocks onto the Earth's surface (Li et al., 2008; Cao et al., 2017), but also released substantial quantities of CO<sub>2</sub> and Hg into the atmosphere. The resulting high atmospheric CO<sub>2</sub> levels ultimately led to global warming (Zhou et al., 2021).

##### 5.4.2. Manganese metallogenesis model

To accurately characterize the paleoredox, paleosalinity, and manganese metallogenic processes of the Datangpo Formation, it is essential consider the paleogeography of the interglacial Nanhua Basin as a restricted margin basin (Wang and Li, 2003). Based on prior paleoenvironmental frameworks (Chen et al., 2008; Li et al., 2012; Yu et al., 2016), a stratified redox model for restricted marginal basins is hereby proposed, wherein anoxic deep waters are overlain by oxic surface waters (Fig. 12). The chemistry of the deep water is primarily influenced by fluctuations in sea level and terrigenous input, which regulate nutrient delivery to the basin and export of organic matter to the deep water. This conceptual model identifies four distinct depositional intervals (I, II, III, and IV), each exhibiting unique geochemical signatures (Fig. 3).

During interval I, corresponding to the Sturtian deglaciation, sea-level rise established a connection between the marginal basin and the open ocean along its southeastern margin (Fig. 1). This hydrographic linkage enabled the nutrient-rich surface waters from the open ocean to flow into the restricted Nanhua Basin, stimulating increased primary

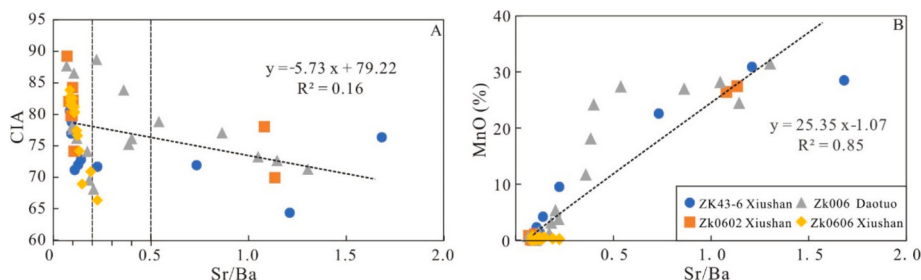


**Fig. 11.** Crossplots of CIA versus Sr/Ba (A) and MnO (%) versus Sr/Ba (B) for samples from the basal Datangpo Formation in Nanhua Basin. The data of ZK43-4 is from Ma et al. (2019), ZK0606 is from Ma et al. (2016), ZK006 is from He et al. (2014), and ZK0602 is from this study. The above-mentioned sections and drill cores are positioned in Fig. 1.

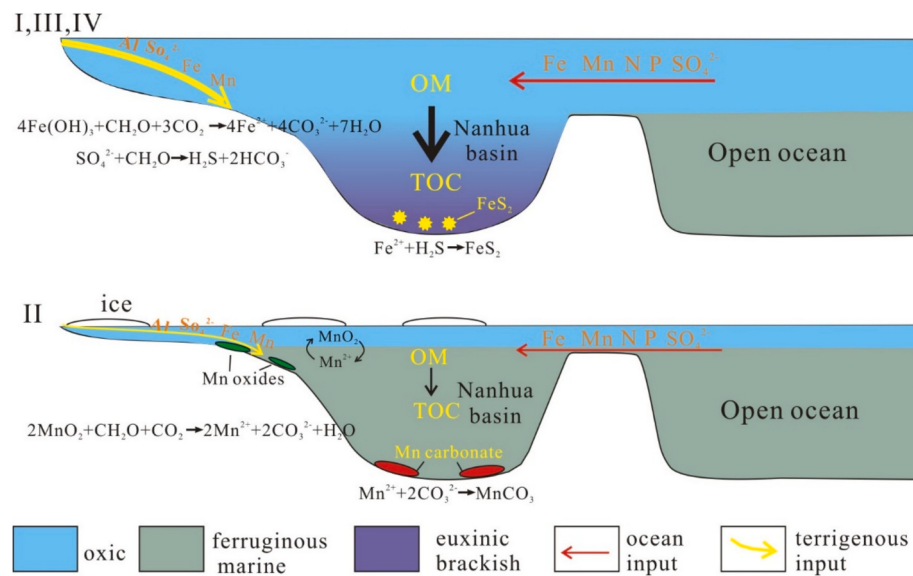


**Fig. 12.** Schematic diagram model of stratified ocean and manganese metallogenesis in the basal Datangpo Formation of the Nanhua Basin. Euxinic and fresh-brackish conditions prevailed in the subsurface waters of the Nanhua Basin during Sturtian deglaciation (I, III, IV); ferruginous and marine conditions emerged during glacier stadial (II), accompanied by the formation of Mn-carbonate.

productivity. Accordingly, the flux of surface-derived organic matter into deeper water layers was enhanced, as evidenced by elevated TOC content. Simultaneously, intensified chemical weathering led to increased terrigenous input, supported by higher value of CIA and decreased Sr/Ba ratios (Fig. 3). Consequently, the euxinic and fresh-brackish conditions developed under abundant supplies of organic matter and enhanced chemical weathering.

The melting of the glaciers is not a constant process, minor ice periods may be interspersed throughout (Qi et al., 2015; Cao et al., 2024). Developing to the interval II, glacier stadials emerging during Sturtian deglaciation likely slowed sea level rise, as evidenced by significantly lower CIA and elevated Sr/Ba ratios (Fig. 3). Concurrently, decreases in U, Mo, and V concentrations, and the  $\text{Fe}_{\text{Py}}/\text{Fe}_{\text{HR}}$  ratio indicate the development of ferruginous conditions in the subsurface waters. However, manganese content increases substantially, accompanied by the formation of abundant rhodochrosite deposits during this interval (Li et al., 2012; Yu et al., 2016).

During interval III, with the ongoing Sturtian deglaciation, eustatic sea levels resumed rising. This is indicated by higher TOC content and an increased nutrient supply from the open ocean, driving elevated primary productivity in the Nanhua Basin's surface waters and enhanced export of organic matter to deeper layers. Concentrations of U, Mo, and V increased and reached peak values, while Mn content decreased significantly, indicating the development of euxinic conditions in bottom waters. Concurrently, higher CIA values and lower Sr/Ba ratios suggest intensified chemical weathering and terrigenous inputs, with the water column reverting to a fresh-brackish environment (Fig. 3).

By interval IV, eustatic sea levels began to decline with the onset of the Marinoan glaciation. Reduced nutrient availability constrained primary productivity and diminished organic matter export to subsurface waters, as evidenced by relatively lower total organic carbon (TOC) contents. However, euxinic water conditions likely persisted, sustained by a dissolved organic carbon (DOC) pool accumulated during interval III when organic matter export fluxes were high. Concentrations of U, Mo, V, and CIA values, along with Sr/Ba ratios, decreased slightly relative to interval III, suggesting the development of moderately euxinic and fresh-brackish conditions in subsurface waters.

The redox state of the open ocean during the Cryogenian interglacial period remains poorly constrained. However, recent studies propose that ferruginous conditions likely prevailed in Neoproterozoic deep

oceans both prior to and following the Cryogenian interglacial interval (Canfield et al., 2008; Li et al., 2008; Song et al., 2017; Li et al., 2020).

Due to the inconsistency in the solubility of  $\text{Mn}^{4+}$  and  $\text{Mn}^{2+}$  species, Manganese exhibits an active biogeochemical cycle across redox boundaries, which may occur above, at, or below the sediment–water interface (Canfield et al., 1993). Hartmann (1964) proposed that manganese is leached from sediments by anoxic pore waters and reoxidized in oxic waters. Manganese oxides can be transported from shallow waters to deeper waters by currents, where manganese is ultimately precipitated as rhodochrosite under reduced alkaline conditions. High levels of Mn carbonate precipitation are also associated with prolonged periods of slightly oxygenated waters in the Landsort Deep of the central Baltic Sea (Häusler et al., 2018). The small standard deviation ( $\sim 1.0 \text{ } \%$ ) of  $\delta^{13}\text{C}_{\text{car}}$  values suggests that the rhodochrosite is likely precipitated near the sediment–water interface under dysoxic conditions, rather than in closed pore water within sediments (Chen et al., 2008; Wang et al., 2024).

In large areas of the Nanhua Basin, anoxic bottom waters drive the leaching of manganese from sediments, leading to elevated concentrations of dissolved  $\text{Mn}^{2+}$ . During Interval II, the emergence of glacial stadials—indicated by significantly lower CIA values and higher Sr/Ba ratios—causes sea-level decline. This shift oxidizes dissolved  $\text{Mn}^{2+}$  to particulate manganese oxides, which accumulate as fine-grained particles in deep sub-basins. As anoxic conditions are re-established, manganese oxides redissolve to release  $\text{Mn}^{2+}$  through the anaerobic oxidation of organic matter,  $\text{H}_2\text{S}$ , and iron sulfides (Canfield et al., 1993). Microbial sulfate reduction results in high alkalinity (Berner et al., 1970), and when combined with elevated  $\text{Mn}^{2+}$  concentrations—potentially reaching supersaturation with respect to rhodochrosite—promotes the precipitation of manganese as rhodochrosite (Huckriede and Meischner, 1996). Therefore, multiple fluctuations in redox state and salinity conditions are critical drivers of manganese enrichment and rhodochrosite formation.

In aquatic systems, electron acceptors in the water column and sediments are consumed following a specific priority sequence:  $\text{O}_2 \rightarrow \text{NO}_3^- \rightarrow \text{Mn}^{4+} \rightarrow \text{Fe}^{3+} \rightarrow \text{SO}_4^{2-}$ . This sequence is coupled with a corresponding reduction in the degradability of residual organic matter at a certain depth (Bo, 2006). This decrease is attributed to the varying degradation characteristics of different types of organic carbon at specific depth (Westrich and Berner, 1984).

Organic matter is essential for the consumption of oxygen and other oxidants, as well as supporting subsequent microbial sulfate reduction (Scott et al., 2008). The co-occurrence of euxinia and reduced salinity in the Cryogenian Nanhua Basin indicates that sulfate was predominantly derived from continental weathering (via riverine inputs) rather than the open ocean (Cheng et al., 2021). This finding aligns with the inference that continental weathering constituted a primary source of sulfate to marginal seas throughout the late Neoproterozoic–Cambrian interval (Li et al., 2020). During intervals I and III, Sturtian deglaciation triggered rising temperatures and enhanced chemical weathering, increasing terrigenous input to the basin and reducing water-column salinity. Concurrently, elevated nutrient inputs from both open-ocean and terrigenous sources fueled high surface-water primary productivity and anaerobic mineralization of organic matter in the water column, inducing sulfidation of bottom waters. Under these conditions, sulfate reduction facilitated pyrite formation. In contrast, during Interval II—marked by the emergence of glacial stadials within the interglacial period—chemical weathering weakened, terrigenous input diminished, and basin water salinity rose to marine levels. Reduced nutrient inputs from both oceanic and terrestrial sources led to decreased primary productivity, reduced downward flux of organic matter and sulfate, and a shift toward manganese reduction as the dominant organic matter oxidation pathway. Under ferruginous conditions, this process promoted rhodochrosite precipitation near the water–sediment interface (Fig. 12).

## 6. Conclusions

- (1) Sedimentological and geochemical proxies consistently indicate that the lower part of black shales of Datangpo Formation (Xiushan, Chongqing) was primarily deposited in euxinic and fresh-brackish conditions. Four distinct depositional intervals (I, II, III, and IV) have been identified in detail, each exhibiting unique water-column chemical signatures. Notably, ferruginous marine interval II, sandwiched between the two euxinic fresh-brackish intervals (I and III), shows a close association with manganese mineralization.
- (2) A stratified redox model is herein proposed to explain the marine chemical condition and manganese mineralization in the semi-restricted Cryogenian Nanhua Basin. The subsurface water chemistry is primarily influenced by sea level fluctuations and terrigenous input, which regulate nutrient delivery to the marginal basin, the redox and salinity condition of subsurface water.
- (3) During intervals II, the onset of glacial stadials within the interglacial period triggered weakened chemical weathering, reduced terrigenous input, and a rise in basin water salinity to marine levels. Diminished nutrient inputs from both open-ocean and terrigenous sources led to decreased primary productivity, reduced downward flux of organic matter and sulfate, and a shift toward manganese reduction as the dominant organic matter oxidation pathway. Under ferruginous conditions, this process facilitated rhodochrosite precipitation near the water–sediment interface.

## CRediT authorship contribution statement

**Zhixin Ma:** Writing – review & editing, Writing – original draft, Resources, Investigation, Formal analysis, Data curation, Conceptualization. **Yun Ling:** Investigation. **Yongjun Qin:** Resources, Investigation. **Yu Liu:** Resources. **Xicai Yao:** Investigation. **Ping Wang:** Writing – review & editing. **Xiting Liu:** Writing – review & editing.

## Declaration of competing interest

The authors declare that they have no known competing financial interests or personal relationships that could have appeared to influence the work reported in this paper.

## Acknowledgments

We extend our gratitude to Shaizhen Xie, Jian Liu, and Liang Guo for their invaluable contributions during the field expeditions. We also express our appreciation to Zihu Zhang and Guodong Xu for their dedicated laboratory assistance. This research is supported by Open Fund of Engineering Technology Innovation Center of Mineral Resources Explorations in Bedrock Zones, Ministry of Natural Resources (No. MREBZ-2023-OF01) Project, NSFC (Natural Science Foundation of China) Project (No. 42202111), Key Scientific Research Project of Colleges and Universities in Henan Province, China (No. 24A170019) and the Fundamental Research Funds for the Universities of Henan Province (No. NSFRF2502121).

## Appendix A. Supplementary data

Supplementary data to this article can be found online at <https://doi.org/10.1016/j.palaeo.2025.113212>.

## Data availability

The authors confirm that all data necessary for supporting the scientific findings of this paper have been provided.

## References

- Ai, J., Zhong, N., Zhang, T., Zhang, Y., Wang, T., George, S., 2021. Oceanic water chemistry evolution and its implications for post-glacial black shale formation: Insights from the Cryogenian Datangpo Formation, South China. *Chem. Geol.* 566, 120083.
- Algeo, T.J., Lyons, T.W., 2006. Mo-total organic carbon covariation in modern anoxic marine environments: implications for analysis of paleoredox and paleohydrographic conditions. *Paleoceanography* 21 (21), 279–298.
- Algeo, T.J., Rowe, H., 2012. Paleceanographic applications of trace-metal concentration data. *Chem. Geol.* 324–325, 6–18.
- Algeo, T.J., Tribouillard, N., 2009. Environmental analysis of paleceanographic systems based on molybdenum–uranium covariation. *Chem. Geol.* 268 (3), 211–225.
- Anbar, A.D., Knoll, A.H., 2002. Proterozoic ocean chemistry and evolution: A bioinorganic bridge. *Science* 297, 1137–1142.
- Bao, X., Zhang, S., Jiang, G., Wu, H., Li, H., Wang, X., An, Z., Yang, T., 2018. Cyclostratigraphic constraints on the duration of the Datangpo Formation and the onset age of the Nantuo (Marinoan) glaciation in South China. *Earth Planet. Sci. Lett.* 483, 52–63.
- Bau, M., Schmidt, K., Koschinsky, A., Hein, J., Kuhn, T., Usui, A., 2014. Discriminating between different genetic types of marine ferro-manganese crusts and nodules based on rare earth elements and yttrium. *Chem. Geol.* 381, 1–9.
- Berner, R.A., Scott, M.R., Thomlinson, C., 1970. Carbonate alkalinity in the porewaters of anoxic marine sediments. *Limnol. Oceanogr.* 15 (4), 544–549.
- Bo, B.J., 2006. *Bacteria and Marine Biogeochemistry*. Springer, Berlin Heidelberg, pp. 169–206.
- Cai, C., Lyons, T.W., Sun, P., Liu, D., Wang, D., Tino, C.J., Luo, G., Peng, Y., Jiang, L., 2022. Enigmatic super-heavy pyrite formation: novel mechanistic insights from the aftermath of the Sturtian Snowball Earth. *Geochim. Cosmochim. Acta* 334, 65–82.
- Canfield, D.E., 2001. Isotope fractionation by natural populations of sulfate-reducing bacteria. *Geochim. Cosmochim. Acta* 65 (7), 1117–1124.
- Canfield, D.E., Raiswell, R., Westrich, J.T., Reaves, C.M., Berner, R.A., 1986. The use of chromium reduction in the analysis of reduced inorganic sulfur in sediments and shales. *Chem. Geol.* 54 (1–2), 149–155.
- Canfield, D.E., Thamdrup, B., Hansen, J.W., 1993. The anaerobic degradation of organic matter in Danish coastal sediments: iron reduction, manganese reduction, and sulfate reduction. *Geochim. Cosmochim. Acta* 57 (16), 3867.
- Canfield, D.E., Poulet, S.W., Knoll, A.H., Narbonne, G.M., Ross, G., Goldberg, T., Strauss, H., 2008. Ferruginous conditions dominated later neoproterozoic deep-water chemistry. *Science* 321 (5891), 949–952.
- Cao, W., Lee, C.-T., Lackey, J., 2017. Episodic nature of continental arc activity since 750 Ma: a global compilation. *Earth Planet. Sci. Lett.* 461, 85–95.
- Cao, G., Liu, Y., Li, C., Peng, P.A., Hou, M., Lash, G.G., Zhou, X., Li, Y., Song, Y., 2023. Salinity variations of the inner Yangtze Sea during the Ordovician–Silurian transition and its influences on marginal marine euxinia. *Glob. Planet. Chang.* 225, 104129.
- Cao, G., Zhang, G., Zhao, Y., Wang, T., Liu, Y., Li, Q., Guo, X., Zhang, Z., Yang, L., Liu, S., Yang, J., Wei, H., 2024. Climatic-hydrologic influence on redox condition in the Cryogenian interglacial Nanhua Basin: insights from the Datangpo Formation in the northwestern Yangtze Block, South China. *Precambrian Res.* 412, 107557.
- Chen, X., Li, D., Ling, H.F., Jiang, S.Y., 2008. Carbon and sulfur isotopic compositions of basal Datangpo Formation, northeastern Guizhou, South China: implications for depositional environment. *Prog. Nat. Sci.* 18 (4), 421–429.

- Cheng, M., Li, C., Chen, X., Zhou, L., Algeo, T.J., Ling, H.F., Feng, L.J., Jin, C.S., 2018. Delayed Neoproterozoic oceanic oxygenation: evidence from Mo isotopes of the Cryogenian Datangpo Formation. *Precambrian Res.* 319, 187–197.
- Cheng, M., Zhang, Z., Liu, S., Liu, X., Wang, H., Chang, B., Jin, C., Pan, W., Cao, M., Li, C., 2021. Hydrological controls on marine chemistry in the Cryogenian Nanhua Basin (South China). *Earth Sci. Rev.* 218, 103678.
- Chu, X., Zhang, Q., Zhang, T., Feng, L., 2003. Sulfur and carbon isotopic variations in neoproterozoic sedimentary rocks from southern China. *Prog. Nat. Sci.* 13 (11), 875–880.
- Clarkson, M.O., Poulton, S.W., Guilbaud, R., Wood, R.A., 2014. Assessing the utility of Fe/Al and Fe-speciation to record water column redox conditions in carbonate-rich sediments. *Chem. Geol.* 382 (11), 111–122.
- Cui, H., Kitajima, K., Spicuzza, M., Fournelle, J., Denny, A., 2018. Questioning the biogenicity of neoproterozoic superheavy pyrite by SIMS. *Am. Mineral.* 103, 1362–1400.
- Dickmann, B., Kuhn, G., Rachold, V., Abelmann, A., Brathauer, U., Fütterer, D.K., Gersonne, R., Grobe, H., 2000. Terrigenous sediment supply in the Scotia Sea (Southern Ocean): response to late Quaternary ice dynamics in Patagonia and on the Antarctic Peninsula. *Palaeogeogr. Palaeoclimatol. Palaeoecol.* 162 (3), 357–387.
- DOBZINSKI, N., Bahlburg, H., Strauss, H., Zhang, Q.R., 2004. Geochemical climate proxies applied to the neoproterozoic glacial succession on the Yangtze Platform, South China. In: Jenkins, G.S., Mcmenamin, M.A.S., McKay, C.P., Sohl, L. (Eds.), *The Extreme Proterozoic: Geology, Geochemistry, and Climate*, Vol. 146. American Geophysical Union, Washington, D. C., pp. 13–32.
- Drummond, J.B.R., Pufahl, P.K., Porto, C.G., Carvalho, M.D.S., 2016. Neoproterozoic peritidal phosphorite from the Sete Lagoas Formation (Brazil) and the Precambrian phosphorus cycle. *Sedimentology* 62 (7), 1978–2008.
- Feng, L., Chu, X., Huang, J., Zhang, Q., Chang, H., 2010. Reconstruction of paleo-redox conditions and early sulfur cycling during deposition of the Cryogenian Datangpo Formation in South China. *Gondwana Res.* 18 (4), 632–637.
- Fike, D.A., Bradley, A.S., Rose, C.V., 2015. Rethinking the ancient sulfur cycle. *Annu. Rev. Earth Planet. Sci.* 43 (1), 593–622.
- Grey, K., Walter, M.R., Calver, C.R., 2003. Neoproterozoic biotic diversification: snowball Earth or aftermath of the Acraman impact? *Geology* 31 (5), 459–462.
- Halverson, G., Porter, S., Shields, G., 2020. The tonian and cryogenian periods. In: Gradstein, F.M., Ogg, J.G. (Eds.), *Geologic Time Scale*. M. D. Schmitz and G. M. Ogg Elsevier, pp. 495–519.
- Hartmann, M., 1964. Zur Geochemie von Mangan und Eisen in der Ostsee. *Meyniana* 14 (53), 3–20.
- Häusler, K., Dellwig, O., Schnetger, B., Feldens, P., Leipe, T., Moros, M., Pollehne, F., Schönke, M., Wegwerth, A., Arz, H.W., 2018. Massive Mn carbonate formation in the Landsort deep (Baltic Sea): Hydrographic conditions, temporal succession, and Mn budget calculations. *Mar. Geol.* 395, 260–270.
- He, Z.W., Yang, R.D., Gao, J.B., Cheng, W., Liu, S., 2014. The geochemical characteristics and sedimentary environment of manganese-bearing rock series of Daotuo manganese deposit, Songtao county of Guizhou province. *Geol. Rev.* 60 (5), 1061–1075 (in Chinese with English abstract).
- Hein, J., Gibbs, A., Clague, D., Torresan, Michael, 1996. Hydrothermal mineralization along submarine rift zones, Hawaii. *Mar. Geotechnol.* 14 (2), 177–203.
- Hoffman, P.F., Kaufman, A.J., Halverson, G.P., Schrag, D.P., 1998. A neoproterozoic snowball earth. *Science* 281 (5381), 1342–1346.
- Hoffman, P.F., Abbot, D.S., Ashkenazy, Y., Benn, D.I., Brocks, J.J., Cohen, P.A., 2017. Snowball earth climate dynamics and cryogenian geology-geobiology. *Sci. Adv.* 3 (11), e1600983.
- Hoshino, Y., Poshbaeva, A., Meredith, W., Snape, C., Poshbaev, V., Versteegh, G., Kuznetsov, N., Leider, A., Van, L.M., Neumann, M., 2017. Cryogenian evolution of stigmasteroid biosynthesis. *Sci. Adv.* 3 (9), 1–7.
- Huckriede, H., Meischner, D., 1996. Origin and environment of manganese-rich sediments within black-shale basins. *Geochim. Cosmochim. Acta* 60 (8), 1399–1413.
- Jin, C., Li, C., Algeo, T.J., Planavsky, N.J., Cui, H., Yang, X., Zhao, Y., Zhang, X., Xie, S., 2016. A highly redox-heterogeneous ocean in South China during the early Cambrian (~529–514 Ma): implications for biota-environment co-evolution. *Earth Planet. Sci. Lett.* 441, 38–51.
- Jørgensen, B.B., Böttcher, M.E., Lüsch, H., Neretin, L.N., Volkov, I.I., 2004. Anaerobic methane oxidation and a deep H<sub>2</sub>S sink generate isotopically heavy sulfides in Black Sea sediments 1 Associate editor: D E. Canfield. *Geochim. Cosmochim. Acta* 68 (9), 2095–2118.
- Kah, L.C., Lyons, T.W., Frank, T.D., 2004. Low marine sulphate and protracted oxygenation of the proterozoic biosphere. *Nature* 431 (7010), 834–838.
- Keigwin, L.D., Gorbarenko, S.A., 1992. Sea level, surface salinity of the Japan Sea, and the Younger Dryas event in the northwestern Pacific Ocean. *Quat. Res.* 37 (3), 346–360.
- Kidder, D.L., Krishnaswamy, R., Mapes, R.H., 2003. Elemental mobility in phosphatic shales during concretion growth and implications for provenance analysis. *Chem. Geol.* 198 (3), 335–353.
- Li, R., Chen, J., Zhang, S., Lei, J., Shen, Y., Chen, X., 1999. Spatial and temporal variations in carbon and sulfur isotopic compositions of Sinian sedimentary rocks in the Yangtze platform, South China. *Precambrian Res.* 97 (1), 59–75.
- Li, Z.X., Li, X.-H., Zhou, H., Kinny, P.D., 2002. Grenvillian continental collision in South China: new SHRIMP U-Pb zircon results and implications for the configuration of Rodinia. *Geology* 30 (2), 163–166.
- Li, Z.X., Bogdanova, S.V., Collins, A.S., Davidson, A., De Waele, B., Ernst, R.E., Fitzsimons, I.C.W., Fuck, R.A., Gladkochub, D.P., Jacobs, J., Karlstrom, K.E., Lu, S., Natapov, L.M., Pease, V., Pisarevsky, S.A., Thrane, K., Vernikovsky, V., 2008. Assembly, configuration, and break-up history of Rodinia: a synthesis. *Precambrian Res.* 160 (1–2), 179–210.
- Li, X.H., Li, W.-X., Li, Z.X., Lo, C.H., Wang, J., Ye, M.F., Yang, Y.H., 2009. Amalgamation between the Yangtze and Cathaysia Blocks in South China: constraints from SHRIMP U-Pb zircon ages, geochemistry and Nd-Hf isotopes of the Shuangxiwu volcanic rocks. *Precambrian Res.* 174 (1–2), 117–128.
- Li, C., Love, G.D., Lyons, T.W., Scott, C.T., Feng, L.J., Huang, J., Chang, H.J., Zhang, Q.R., Chu, X.L., 2012. Evidence for a redox stratified Cryogenian marine basin, Datangpo Formation, South China. *Earth Planet. Sci. Lett.* 331, 246–256.
- Li, C., Shi, W., Cheng, M., Jin, C., Algeo, T.J., 2020. The redox structure of Ediacaran and early Cambrian oceans and its controls. *Sci. Bull.* 65 (24), 2141–2149.
- Li, T.B., Maynard, J.B., Alten, J., 2006. Superheavy S isotopes from glacier-associated sediments of the Neoproterozoic of South China: oceanic anoxia or sulfate limitation? *Mem. Geol. Soc. Am.* 198 (198), 205–222.
- Liu, X., Fike, D., Li, A., Dong, J., Xu, F., Zhuang, G., Rendle-Bühring, R., Wan, S., 2019. Pyrite sulfur isotopes constrained by sedimentation rates: evidence from sediments on the East China Sea inner shelf since the late Pleistocene. *Chem. Geol.* 505, 66–75.
- Liu, Z., Ma, Z.X., Liu, W., Ling, Y., 2021a. Sedimentary environment and manganese ore deposits in the Nanhua Period Datangpo Formation in Xiaochayuan Area, Xiushan, Chongqing. *Acta Sedimentol. Sin.* 39 (3), 515–524 (in Chinese with English abstract).
- Liu, X., Zhang, M., Li, A., Fan, D., Dong, J., Jiao, C., Chang, X., Gu, Y., Zhang, K., Wang, H., 2021b. Depositional control on carbon and sulfur preservation onshore and offshore the Oujiang Estuary: implications for the C/S ratio as a salinity indicator. *Cont. Shelf Res.* 227, 104510.
- Love, G.D., Grosjean, E., Stalvies, C., Fike, D.A., Grotzinger, J.P., Bradley, A.S., Kelly, A.E., Bhatia, M., Meredith, W., Snape, C.E., 2009. Fossil steroids record the appearance of demospongiae during the cryogenian period. *Nature* 457 (7230), 718–721.
- Ma, Z.X., Luo, L., Liu, X.T., Liu, W., Sun, Z.M., 2016. Palaeoenvironment of the Datangpo Formation of Nanhua System in Xiaochayuan manganese deposit in Xiushan area of Chongqing. *J. Palaeogeogr.* 18 (1), 473–486 (in Chinese with English abstract).
- Ma, Z., Liu, X., Yu, W., Du, Y., Du, Q., 2019. Redox conditions and manganese metallogenesis in the Cryogenian Nanhua Basin: insight from the basal Datangpo Formation of South China. *Palaeogeogr. Palaeoclimatol. Palaeoecol.* 529, 39–52.
- Matthias, T., Godfrey, J.S., 1994. *Regional Oceanography: An Introduction*. Pergamon Press, Pergamon, pp. 1–422.
- Maynard, J.B., 1992. Chemistry of modern soils as a guide to interpreting precambrian paleosols. *J. Geol.* 100 (3), 279–289.
- Nesbitt, H., Young, G., 1982. Early proterozoic climates and plate motions inferred from major element chemistry of lutites. *Nature* 299 (5885), 715–717.
- Och, L.M., Shields-Zhou, G.A., 2012. The Neoproterozoic oxygenation event: environmental perturbations and biogeochemical cycling. *Earth Sci. Rev.* 110 (1–4), 26–57.
- Paytan, A., Griffith, E.M., 2007. Marine barite: recorder of variations in ocean export productivity. *Deep-Sea Res. II Top. Stud. Oceanogr.* 54 (5), 687–705.
- Peter, J.M., 1996. Mineralogy, bulk and rare earth element geochemistry of massive sulphide-associated hydrothermal sediments of the Brunswick Horizon, Bathurst Mining Camp, New Brunswick. *Can. J. Earth Sci.* 33 (2), 252–283.
- Pierrehumbert, R.T., Abbot, D.S., Voigt, A., Koll, D., 2011. Climate of the neoproterozoic. *Annu. Rev. Earth Planet. Sci.* 39 (1), 417–463.
- Planavsky, N.J., McGoldrick, P., Scott, C.T., Li, C., Reinhard, C.T., Kelly, A.E., Chu, X., Bekker, A., Love, G.D., Lyons, T.W., 2011. Widespread iron-rich conditions in the mid-Proterozoic Ocean. *Nature* 477 (7365), 448–451.
- Poulton, S.W., Canfield, D.E., 2005. Development of a sequential extraction procedure for iron: implications for iron partitioning in continentally derived particulates. *Chem. Geol.* 214 (3–4), 209–221.
- Poulton, S.W., Canfield, D.E., 2011. Ferruginous conditions: a dominant feature of the ocean through earth's history. *Elements* 7 (2), 107–112.
- Qi, L., Yu, W.C., Du, Y.S., Zhou, Q., Guo, H., Wang, J.W., Wang, P., Xu, Y., 2015. Paleoclimate evolution of the Cryogenian Ties'ao Formation-Datangpo formation in East Guizhou Province: evidence from the chemical index of alteration. *Geol. Sci. Technol. Inform.* 34 (6), 47–57 (in Chinese with English abstract).
- Qi, L., Zhang, Y., Jiao, L., Liu, J., Du, Y., Wang, Z., Yu, W., Guo, H., Chen, Q., Wu, W., 2023. Geochemical evolution of the Doushantuo economic phosphorite in Central Guizhou, South China: quantified multi-stage metallogenetic process. *Ore Geol. Rev.* 161, 105647.
- Raiswell, R., Newton, R., Bottrell, S.H., Coburn, P.M., Briggs, D.E.G., Bond, D.P.G., Poulton, S.W., 2008. Turbidite depositional influences on the diagenesis of Beecher's Trilobite Bed and the Hunsrück Slate; sites of soft tissue pyritization. *Am. J. Sci.* 308 (2), 105–129.
- Remírez, M.N., Algeo, T.J., 2020. Paleosalinity determination in ancient epicontinent seas: A case study of the T-OAE in the Cleveland Basin (UK). *Earth-Sci. Rev.* 201, 103072.
- Rooney, A.D., Yang, C., Condon, D.J., Zhu, M.Y., Macdonald, F.A., 2020. U-Pb and Re-Os geochronology tracks stratigraphic condensation in the Sturtian snowball Earth aftermath. *Geology* 48 (6), 625–629.
- Sahoo, S.K., Planavsky, N.J., Jiang, G., Kendall, B., Owens, J.D., Wang, X., Shi, X., Anbar, A.D., Lyons, T.W., 2016. Oceanic oxygenation events in the anoxic Ediacaran Ocean. *Geobiology* 14 (5), 457–468.
- Scott, C., Lyons, T.W., Bekker, A., Shen, Y., Poulton, S.W., Chu, X., Anbar, A.D., 2008. Tracing the stepwise oxygenation of the Proterozoic Ocean. *Nature* 452 (7186), 456–459.
- Song, H., Jiang, G., Poulton, S.W., Wignall, P.B., Tong, J., Song, H., An, Z., Chu, D., Tian, L., She, Z., Wang, C., 2017. The onset of widespread marine red beds and the evolution of ferruginous oceans. *Nat. Commun.* 8 (1), 399.
- Song, H.Y., An, Z., Ye, Q., Stüeken, E.E., Li, J., Hu, J., Algeo, T., Tian, L., Chu, D.L., Song, H.J., Xiao, S., Tong, J., 2023. Mid-latitudinal habitable environment for

- marine eukaryotes during the waning stage of the Marinoan snowball glaciation. *Nat. Commun.* 14, 1564.
- Spence, G.H., Le Heron, D.P., Fairchild, I.J., 2016. Sedimentological perspectives on climatic, atmospheric and environmental change in the Neoproterozoic Era. *Sedimentology* 63 (2), 253–306.
- Taylor, S.R., McLennan, S.M., 1985. The Continental Crust: Its Composition and Evolution, An Examination of the Geochemical Record Preserved in Sedimentary Rocks. Blackwell Scientific Publications, Oxford, pp. 1–312.
- Tribouillard, N., Algeo, T.J., Lyons, T., Riboulleau, A., 2006. Trace metals as paleoredox and paleoproduction proxies: an update. *Chem. Geol.* 232 (1), 12–32.
- Tu, C., Diamond, C.W., Stüeken, E.E., Cao, M., Pan, W., Lyons, T.W., 2024. Dynamic evolution of marine productivity, redox, and biogeochemical cycling track local and global controls on Cryogenian Sea-level change. *Geochim. Cosmochim. Acta* 365, 114–135.
- Ussui, A., Someya, M., 1997. Distribution and composition of marine hydrogenic and hydrothermal manganese deposits in the Northwest Pacific. *Geol. Soc. Lond. Spec. Publ.* 119 (1), 177–198.
- Wang, J., Li, Z.X., 2003. History of Neoproterozoic rift basins in South China: implications for Rodinia break-up. *Precambrian Res.* 122 (1), 141–158.
- Wang, X.C., Li, X.H., Li, W.X., Li, Z.X., 2009. Variable involvements of mantle plumes in the genesis of mid-Neoproterozoic basaltic rocks in South China: a review. *Gondwana Res.* 15 (3–4), 381–395.
- Wang, P., Zhou, Q., Du, Y., Yu, W., Xu, Y., Qi, L., Yuan, L., 2016. Characteristics of pyrite sulfur isotope of Mn deposit from Datangpo Formation in Songtao Area, East Guizhou Province and its geological significance. *Earth Sci. J. China Univ. Geosci.* 41 (12), 2031–2040.
- Wang, P., Du, Y.S., Yu, W.C., Zhou, Q., Xu, Y., Qi, L., Yuan, L.J., Pan, W., 2020. The chemical index of alteration (CIA) as a proxy for climate change during glacial-interglacial transitions in Earth history. *Earth Sci. Rev.* 201, 103032.
- Wang, P., Wang, J., Du, Y., Yu, W., Zhou, Q., Tian, L., Yuan, L., Pan, W., Wei, W., Qin, Y., Ma, Z., 2024. Manganese mineralization constrained by redox conditions in the Cryogenian Nanhua Basin, South China and its implications for nitrogen and carbon cycling. *Front. Mar. Sci.* 11, 1469283.
- Wei, W., Algeo, T.J., 2020. Elemental proxies for paleosalinity analysis of ancient shales and mudrocks. *Geochim. Cosmochim. Acta* 287, 341–366.
- Wei, G.Y., Wei, W., Wang, D., Li, T., Yang, X., Shields, G.A., Zhang, F., Li, G., Chen, T., Yang, T., Ling, H.F., 2020. Enhanced chemical weathering triggered an expansion of euxinic seawater in the aftermath of the Sturtian glaciation. *Earth Planet. Sci. Lett.* 539, 116244.
- Wei, W., Yu, W., Du, Y., Algeo, T.J., Li, Z., Cheng, M., Wang, P., Zhang, J., Robbins, L.J., Konhauser, K., 2024. A new salinity-based model for Cryogenian Mn-carbonate deposits. *Precambrian Res.* 403, 107309.
- Westrich, J.T., Berner, R.A., 1984. The role of sedimentary organic matter in bacterial sulfate reduction: the G model tested. *Limnol. Oceanogr.* 29 (2), 236–249.
- Wu, J., Tan, Z., Jia, W., Chen, J., Peng, P.A., 2024. Nitrogen isotopes and geochemistry of the basal Datangpo Formation: contrasting redox conditions in the upper and lower water columns during the Cryogenian interglaciation period. *Palaeogeogr. Palaeoclimatol. Palaeoecol.* 637, 112005.
- Xiao, J., He, J., Yang, H., Wu, C., 2017. Comparison between Datangpo-type manganese ores and modern marine ferromanganese oxyhydroxide precipitates based on rare earth elements. *Ore Geol. Rev.* 89, 290–308.
- Yan, B., Shen, W., Zhao, N., Zhu, X., 2020. Constraints on the nature of the Marinoan glaciation: cyclic sedimentary records from the Nantuo Formation, South China. *J. Asian Earth Sci.* 189, 104137.
- Ye, Y., Wang, H., Zhai, L., Wang, X., Wu, C., Zhang, S., 2018. Contrasting Mo–U enrichments of the basal Datangpo Formation in South China: implications for the Cryogenian interglacial ocean redox. *Precambrian Res.* 315, 66–74.
- Ye, Y., Wang, X., Wang, H., Fan, H., Chen, Z., Guo, Q., Wang, Z., Wu, C., Canfield, D.E., Zhang, S., 2024. Hydrological dynamics and manganese mineralization in the wake of the Sturtian glaciation. *Geochim. Cosmochim. Acta* 376, 14–24.
- Yu, W., Algeo, T.J., Du, Y., Maynard, B., Guo, H., Zhou, Q., Peng, T., Wang, P., Yuan, L., 2016. Genesis of Cryogenian Datangpo manganese deposit: hydrothermal influence and episodic post-glacial ventilation of Nanhua Basin, South China. *Palaeogeogr. Palaeoclimatol. Palaeoecol.* 459, 321–337.
- Yu, W., Polgári, M., Gyollai, I., Fintor, K., Szabó, M., Kovács, I., Fekete, J., Du, Y., Zhou, Q., 2019. Microbial metallogenesis of Cryogenian manganese ore deposits in South China. *Precambrian Res.* 322, 122–135.
- Zhang, S., Jiang, G., Han, Y., 2008. The age of the Nantuo Formation and Nantuo glaciation in South China. *Terra Nova* 20 (4), 289–294.
- Zhang, F., Zhu, X., Yan, B., Kendall, B., Peng, X., Li, J., Algeo, T.J., Romaniello, S., 2015. Oxygenation of a Cryogenian Ocean (Nanhua Basin, South China) revealed by pyrite Fe isotope compositions. *Earth Planet. Sci. Lett.* 429, 11–19.
- Zhou, Q., Du, Y.S., Yuan, L.J., Zhang, S., Yu, W.C., Yang, S.T., 2016. The Structure of the Wuling Rift Basin and its control on the manganese deposit during the Nanhua period in Guizhou-Hunan-Chongqing border area, South China. *Earth Sci.* 41, 177–188.
- Zhou, T., Pan, X., Sun, R., Deng, C., Shen, J., Kwon, S.Y., Grasby, S.E., Xiao, J., Yin, R., 2021. Cryogenian interglacial greenhouse driven by enhanced volcanism: evidence from mercury records. *Earth Planet. Sci. Lett.* 564, 116902.
- Zhou, Q., Wu, C.L., Hu, X.Y., Yang, B.N., Zhang, X.L., Du, Y.S., 2022. A new metallogenic model for the giant manganese deposits in northeastern Guizhou, China. *Ore Geol. Rev.* 149, 105070.
- Zhu, G., Li, T., Zhang, Z., Zhao, K., Song, H., Wang, P., Yan, H.H., Song, H., 2022. Nitrogen isotope evidence for oxygenated upper ocean during the Cryogenian interglacial period. *Chem. Geol.* 604, 120929.